Cell Reports

Article

The prolyl-isomerase PIN1 is essential for nuclear Lamin-B structure and function and protects heterochromatin under mechanical stress

Graphical abstract

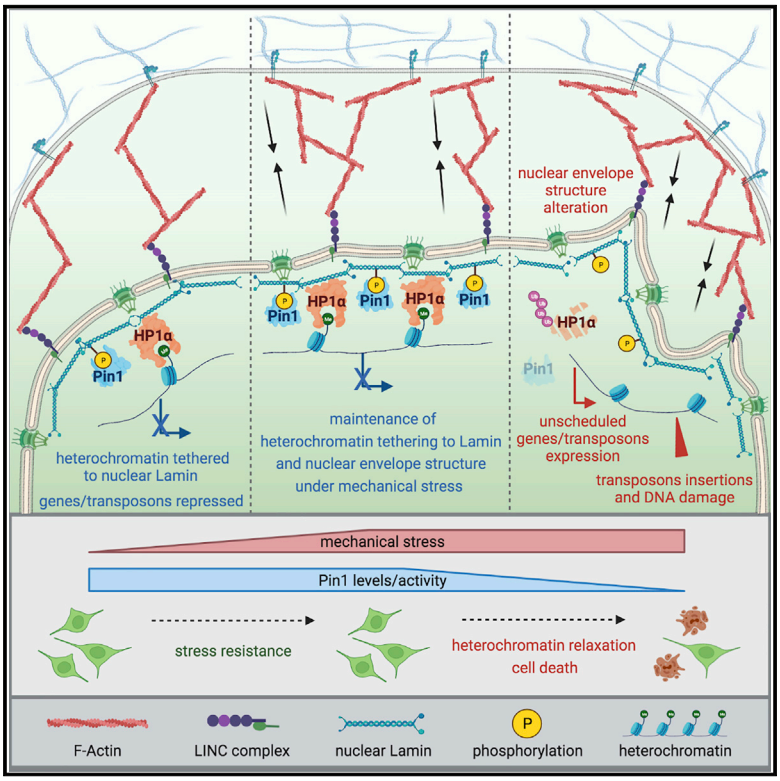

Highlights

- PIN1 stabilizes HP1α in complex with LaminB in a phosphorylation-dependent manner
- PIN1 function maintains nuclear envelope structure under mechanical stress
- PIN1 loss causes HP1α degradation, heterochromatin relaxation, transposon derepression
- Loss of PIN1 nucleo-protective function contributes to Alzheimer's disease

Authors

Francesco Napoletano, Gloria Ferrari Bravo, Ilaria Anna Pia Voto, ..., Fiamma Mantovani, Valeria Specchia, Giannino Del Sal

Correspondence

fnapoletano@units.it (F.N.), gdelsal@units.it (G.D.S.)

In brief

In aging-related diseases, heterochromatin becomes relaxed through poorly understood mechanisms, which makes cells prone to genome damage and death. Napoletano et al. find a mechanism of signal transduction through the nuclear envelope that maintains nuclear architecture and safeguards heterochromatin under mechanical stress and is impaired in neurodegenerative diseases.

Napoletano et al., 2021, Cell Reports *36*, 109694
September 14, 2021
https://doi.org/10.1016/j.celrep.2021.109694

CellPress

Cell Reports

CellPress
OPEN ACCESS

Article

The prolyl-isomerase PIN1 is essential for nuclear Lamin-B structure and function and protects heterochromatin under mechanical stress

Francesco Napoletano,[1,2,9,10,*] Gloria Ferrari Bravo,[1,2,9,10] Ilaria Anna Pia Voto,[1] Aurora Santin,[1] Lucia Celora,[1] Elena Campaner,[1,2,9] Clara Dezi,[2,9] Arianna Bertossi,[1,2,9] Elena Valentino,[1] Mariangela Santorsola,[1,2] Alessandra Rustighi,[1,2,9] Valentina Fajner,[3] Elena Maspero,[3] Federico Ansaloni,[4] Valeria Cancila,[5] Cesare Fabio Valenti,[5] Manuela Santo,[4] Osvaldo Basilio Artimagnella,[4] Sara Finaurini,[4] Ubaldo Gioia,[3] Simona Polo,[3] Remo Sanges,[4] Claudio Tripodo,[3,5] Antonello Mallamaci,[4] Stefano Gustincich,[4,6] Fabrizio d'Adda di Fagagna,[3,7] Fiamma Mantovani,[1,2,9] Valeria Specchia,[8] and Giannino Del Sal[1,2,3,9,11,*]

[1]Laboratorio Nazionale CIB (LNCIB), Area Science Park, Padriciano 99, 34149 Trieste, Italy
[2]Department of Life Sciences (DSV), University of Trieste, 34127 Trieste, Italy
[3]FIRC Institute of Molecular Oncology (IFOM), 20139 Milan, Italy
[4]Area of Neuroscience, International School for Advanced Studies (SISSA), 34146 Trieste, Italy
[5]Tumor Immunology Unit, Department of Health Science, Human Pathology Section, School of Medicine, University of Palermo, 90133 Palermo, Italy
[6]Central RNA Laboratory, Italian Institute of Technology, 16163 Genova, Italy
[7]Institute of Molecular Genetics, National Research Institute (CNR), Pavia, Italy
[8]Department of Biological and Environmental Sciences and Technologies (DiSTeBA), University of Salento, 73100 Lecce, Italy
[9]Present address: International Centre for Genetic Engineering and Biotechnology (ICGEB), 34149 Trieste, Italy
[10]These authors contributed equally
[11]Lead contact
*Correspondence: fnapoletano@units.it (F.N.), gdelsal@units.it (G.D.S.)
https://doi.org/10.1016/j.celrep.2021.109694

SUMMARY

Chromatin organization plays a crucial role in tissue homeostasis. Heterochromatin relaxation and consequent unscheduled mobilization of transposable elements (TEs) are emerging as key contributors of aging and aging-related pathologies, including Alzheimer's disease (AD) and cancer. However, the mechanisms governing heterochromatin maintenance or its relaxation in pathological conditions remain poorly understood. Here we show that PIN1, the only phosphorylation-specific *cis/trans* prolyl isomerase, whose loss is associated with premature aging and AD, is essential to preserve heterochromatin. We demonstrate that this PIN1 function is conserved from *Drosophila* to humans and prevents TE mobilization-dependent neurodegeneration and cognitive defects. Mechanistically, PIN1 maintains nuclear type-B Lamin structure and anchoring function for heterochromatin protein 1α (HP1α). This mechanism prevents nuclear envelope alterations and heterochromatin relaxation under mechanical stress, which is a key contributor to aging-related pathologies.

INTRODUCTION

Heterochromatin (HC) plays a crucial role in eukaryotic cell functions, and its alteration has been proposed as a key mechanism in aging and aging-related diseases, including Alzheimer's disease (AD) and cancer (Zhang et al., 2020). In almost all higher eukaryotes, including humans, HC mainly comprises satellite repeats and transposable elements (TE), classified as retrotransposons (class I TEs) and DNA transposons (class II TEs). Retrotransposons, whose mobilization requires reverse transcription by a self-encoded reverse transcriptase, comprise endogenous retrovirus (ERV; harboring long terminal repeats [LTRs]) long interspersed nuclear element (LINE) and short interspersed nuclear element (SINE) families. In humans, TEs occupy more than half of the genome, and about 100 LINE L1 copies are full length and competent for mobilization (Payer and Burns, 2019).

TE mobilization is a source of genetic variation with the potential to contribute to evolution but also to generate harmful mutations (Payer and Burns, 2019; Specchia et al., 2010). Unscheduled TE expression and mobilization, accompanied by DNA damage, have been associated with manifestations of physiological and premature aging, including neuronal and retina degeneration and reduced fertility, and have been shown to contribute to aging-related diseases, such as AD and cancer (Li et al., 2013; Kaneko et al., 2011; Zamudio and Bourc'his, 2010; Guo et al., 2018; Sun et al., 2018; Payer and Burns, 2019).

In concert with DNA methylation and transcriptional and post-transcriptional silencing by small interfering RNA (siRNA) and piwi-interacting RNA (piRNA) pathways (mainly active in somatic tissue and the germline, respectively), HC is crucial to restrain TE expression and mobilization (Allshire and Madhani, 2018a). HC organization involves multiple mechanisms, including protein

post-translational modifications (PTMs) and tethering to the nuclear envelope (NE) (Hildebrand and Dekker, 2020), a double membrane structure stabilized by a meshwork of Lamin proteins. Lamins are connected to the cytoskeleton and the extracellular environment through the linker of nucleoskeleton and cytoskeleton (LINC) complex. This allows sensing and adaptation of NE structure/function, chromatin organization, and gene expression to mechanical cues (Kirby and Lammerding, 2018), and recent evidence has shown that cells protect the genome from mechanical challenge impinging on the nucleus (Cho et al., 2019; Kidiyoor et al., 2020; Kumar et al., 2014; Nava et al., 2020). At the NE, HC forms Lamin-associated domains (LADs), enriched in HC protein 1α (HP1α) bound to di/trimethylated K9 histone H3 (H3K9me2/3), so that genes and TEs in these regions are transcriptionally repressed (Guelen et al., 2008; Pindyurin et al., 2018). LADs are, in fact, enriched in and essential for the repression of L1s (Vazquez et al., 2019).

Interestingly, in AD, dysfunctional TAU protein has been shown to cause mechanical stress altering the NE (Frost et al., 2016), HP1α reduction (Frost et al., 2014), and TE hyperactivity (Guelen et al., 2008; Sun et al., 2018). This suggests that HC maintenance in response to mechanical cues may prevent TE deleterious effects. However, how mechanisms of HC organization at the NE are regulated and how mechanical cues affect TEs remains largely unknown.

PIN1 is the only known enzyme that *cis-trans* isomerizes prolines within the phosphorylated Ser/Thr-Pro (pS/T-P) motif. This results in substrate conformational changes affecting stability, interactions, localization, and function. In this way, PIN1 regulates multiple cellular processes, including some associated with TE regulation, such as chromatin state, transcription, and DNA damage repair (Zannini et al., 2019). Several diseases have been associated with altered PIN1 function. Although increased PIN1 levels are frequent in cancer and correlate to a poor prognosis (Girardini et al., 2014; Rustighi et al., 2009, 2014; Zhou and Lu, 2016), reduced PIN1 expression and activity are associated with AD (Lu et al., 1999; Pastorino et al., 2006), and *Pin1* knockout mice ($Pin1^{-/-}$) display premature aging phenotypes, including neurodegeneration, retina degeneration and reduced fertility (Atchison et al., 2003; Liou et al., 2002, 2003). Similar phenotypes have been associated with unscheduled TE expression and mobilization (Kaneko et al., 2011; Zamudio and Bourc'his, 2010; Guo et al., 2018; Sun et al., 2018).

Here we show that PIN1 is essential to preserve HC, a function that prevents TE mobilization-dependent neurodegeneration and cognitive defects. We provide evidence that PIN1 maintains nuclear type-B Lamin structure and anchoring function for HP1α and that this mechanism prevents NE alterations and HC relaxation under mechanical stress, an emerging contributor to aging-related diseases.

RESULTS

Dodo/PIN1 preserves tissue homeostasis in *Drosophila*

To study the role of PIN1 in regulating TEs, we used *Drosophila melanogaster* as a model organism in which silencing mechanisms of TE activity have been established (McCullers and Steiniger, 2017). All experiments, unless otherwise stated, were performed in 4-day-old adult flies. In wild-type (WT) brain and ovaries, in which TE silencing is crucial for tissue homeostasis, protein expression of the PIN1 ortholog Dodo was ubiquitous and partially overlapped with type B Lamin Dm0 (LamB) in the nucleus (Figures S1A–S1C). In the WT brain, Dodo protein levels declined slightly with age (Figure 1A), whereas cells positive for Terminal deoxynucleotidyl transferase dUTP nick end labeling (TUNEL) accumulated (Figure 1B). To assess the role of Dodo in tissue homeostasis, we used *dodo* mutant (harboring the P element insertion $dodo^{EY03779}$) and $dodo^{RNAi}$-expressing flies, which both displayed a strong reduction of Dodo protein levels in the brain and ovaries compared with controls (Figures 1A and S1C–S1E). Neuron-specific $dodo^{RNAi}$ accelerated TUNEL-positive cell accumulation (Figure 1B), accompanied by cognitive (Figure 1C) and motor (Figure S1F) defects, and *dodo* mutant flies displayed similar cognitive defects (Figure 1C). Furthermore, a reduction of Dodo protein levels was associated with retina degeneration (Figure S1G) and reduced fertility (Figure S1H), as also observed in $Pin1^{-/-}$ mice (Atchison et al., 2003; Liou et al., 2002). We also generated transgenic flies expressing human *PIN1* (*hPIN1*) (Figure S1I), which suppressed neurodegeneration (Figure 1B) and motor defects (Figure S1F) caused by $dodo^{RNAi}$.

These results demonstrate that Dodo has a fundamental role in preserving tissue function.

Dodo restrains the activity of TEs

To unveil transcriptional alterations underlying the observed phenotypes, we performed RNA sequencing (RNA-seq) in fly heads. *dodo* mutation was associated with altered RNA levels of membrane remodeling (in particular components of the endosomal sorting complex required for transport - ESCRT - III complex), innate immunity, and translation genes (Figures 2A and S2A; Table S1), and especially of several TEs, mostly upregulated LTRs and LINE-like retrotransposons, according to locus-specific (Figure 2A; Table S1) and consensus analyses (Figure S2B; Table S1). Upregulation of representative TE RNAs was validated by qPCR in *dodo* mutant (Figure S2C) and $dodo^{RNAi}$-expressing fly heads (Figure 2B), and similar results were obtained in ovaries (Figure S2C). Also, *hPIN1* expression suppressed TE RNA upregulation in $dodo^{RNAi}$ fly heads (Figure 2C). These results prove that Dodo is a negative regulator of TE expression. This function was independent of the microtubule-associated protein dTAU, whose human ortholog (hTAU) is regulated by PIN1 (Liou et al., 2003) and linked to TE induction (Guelen et al., 2008; Sun et al., 2018), because $dTAU^{RNAi}$ did not modify TE expression in $dodo^{RNAi}$ fly heads (Figures 2B and S2D).

Importantly, neurological defects caused by Dodo reduction were associated with increased genomic copy numbers of representative TEs (Figure 2D) and with DNA damage in the brain, as shown by COMET assay (Figure 2E) and γH2Av quantification (Figure 2F). These phenotypes, including TUNEL-positive cell appearance and cognitive defects, were suppressed by feeding flies the reverse transcriptase inhibitor 3TC (also known as lamivudine) (Figures 2D and 2F–2H), a drug reported previously to impair retrotransposon mobilization (Sun et al., 2018).

These results demonstrate that Dodo has a fundamental function in restraining TE activity, preserving brain neuron survival and cognitive performance.

CellPress
OPEN ACCESS

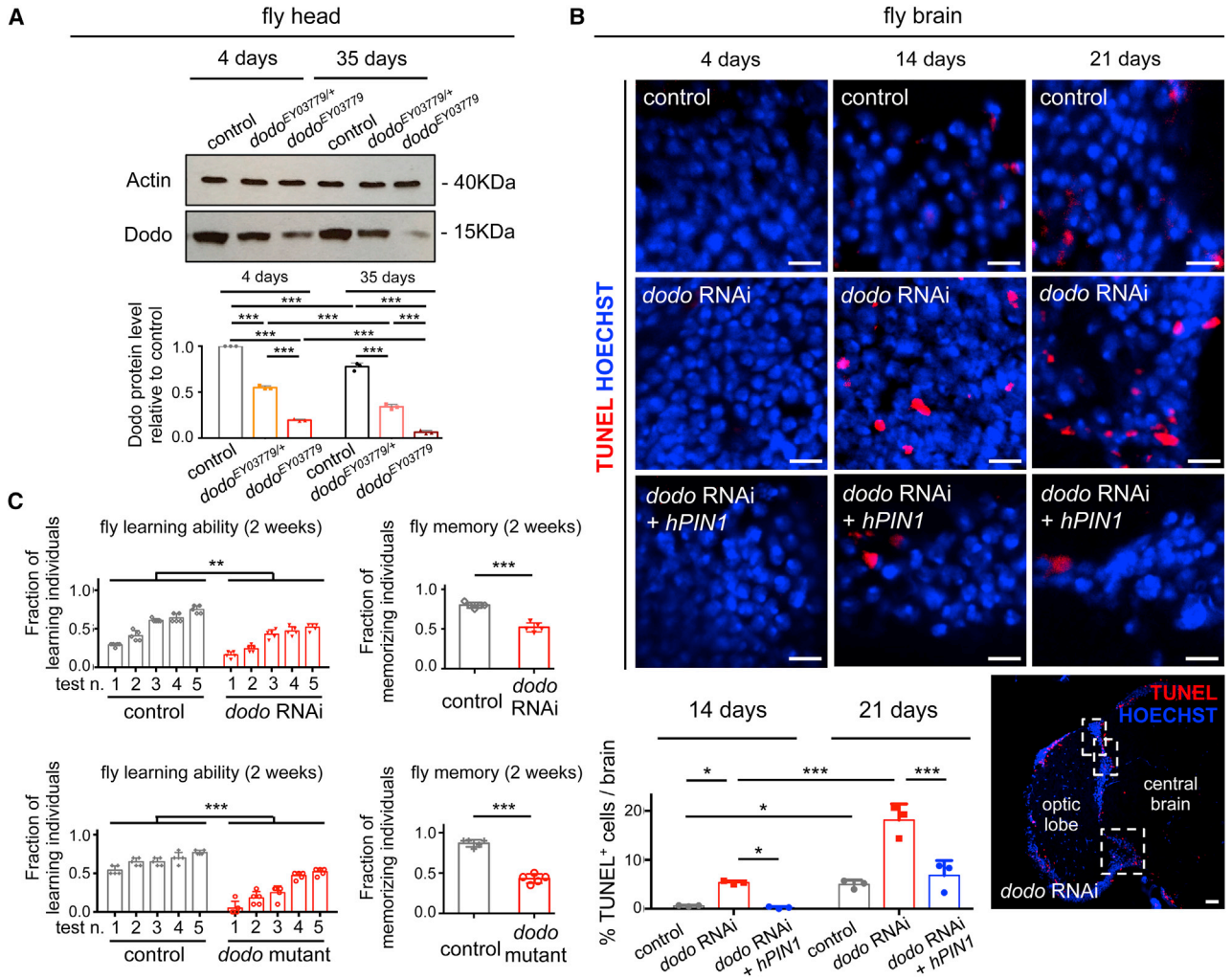

Figure 1. Dodo maintains brain neurons healthy aging

(A) Western blot analysis of Dodo in WT control, *dodo*$^{EY03779/+}$ heterozygous, and *dodo*^{EY03779} homozygous flies. Actin was used as reference for quantifications, showing mean values ± SD of n = 3 biological replicates. ***p < 0.001 by two-way ANOVA with Tukey correction.

(B) TUNEL in cryosections of control (*Elav-GAL4*) flies and flies expressing *dodo* RNAi (*Elav* > *dodo*^{KK108535}) or *dodo* RNAi and *hPIN1* (*Elav* > *dodo*^{KK108535} > *hPIN1*). Nuclei are stained with Hoechst. Quantifications show mean values ± SD of n = 3 individuals (200–400 cells/individual). ***p < 0.001, *p < 0.05 by two-way ANOVA with Tukey correction. In the bottom right panel, fly brain regions sampled (dashed squares), central brain and optic lobe are indicated. Scale bars, 5 μm.

(C) Learning (left panels) and memory (right panels) assays in 2-week-old control (*Elav-GAL4*) and *dodo* RNAi (*Elav* > *dodo*^{KK108535}) (top panels) and in 2-week-old WT control and *dodo*^{EY03779} mutant (bottom panels) flies. For learning assays, values represent mean ± SD of n = 5 groups (n = 20 individuals/group). For each group, flies positive for phototaxis were iteratively trained five times (test n. 1–5) for the ability to associate light with a negative stimulus (0.1 M quinine solution, bitter taste) that inhibits phototaxis (aversive learning). For each test, the fractions of individuals positive (unlearned) and negative (learning) for phototaxis were calculated. ***p < 0.001, **p < 0.01 by two-way ANOVA with Tukey correction. For short-term memory assays, values represent mean ± SD of an n = 20 individuals group. Single groups of trained flies were left for 5 h at 25°C and re-tested. The fractions of individuals positive (memory defective) and negative (memorizing) for phototaxis were calculated. ***p < 0.001 by two-tailed unpaired Student's t test.

See also Figure S1.

Dodo maintains HC

We next assessed whether loss of Dodo could lead to TE expression through HC alteration. We mapped genes and TEs, differentially expressed in *dodo* mutant versus WT fly head RNA-seq, on chromatin states, using genome coordinates from DamIDseq (DNA adenine methyltransferase identification-sequencing) experiments that identified constitutive and facultative HC loci in fly brain neurons (Marshall and Brand, 2017). According to these experiments, genes and TEs are distributed across all chromatin states, including repressive HP1a (the ortholog of HP1α), a key factor in HC formation (James and Elgin, 1986), and Polycomb group (PcG), active Tritorax group (TrxG), and Black (lacking common histone modifications or known histone-code readers/writers) chromatin. Statistical analysis highlighted that genes and TEs upregulated in the *dodo* mutant were overrepresented in the

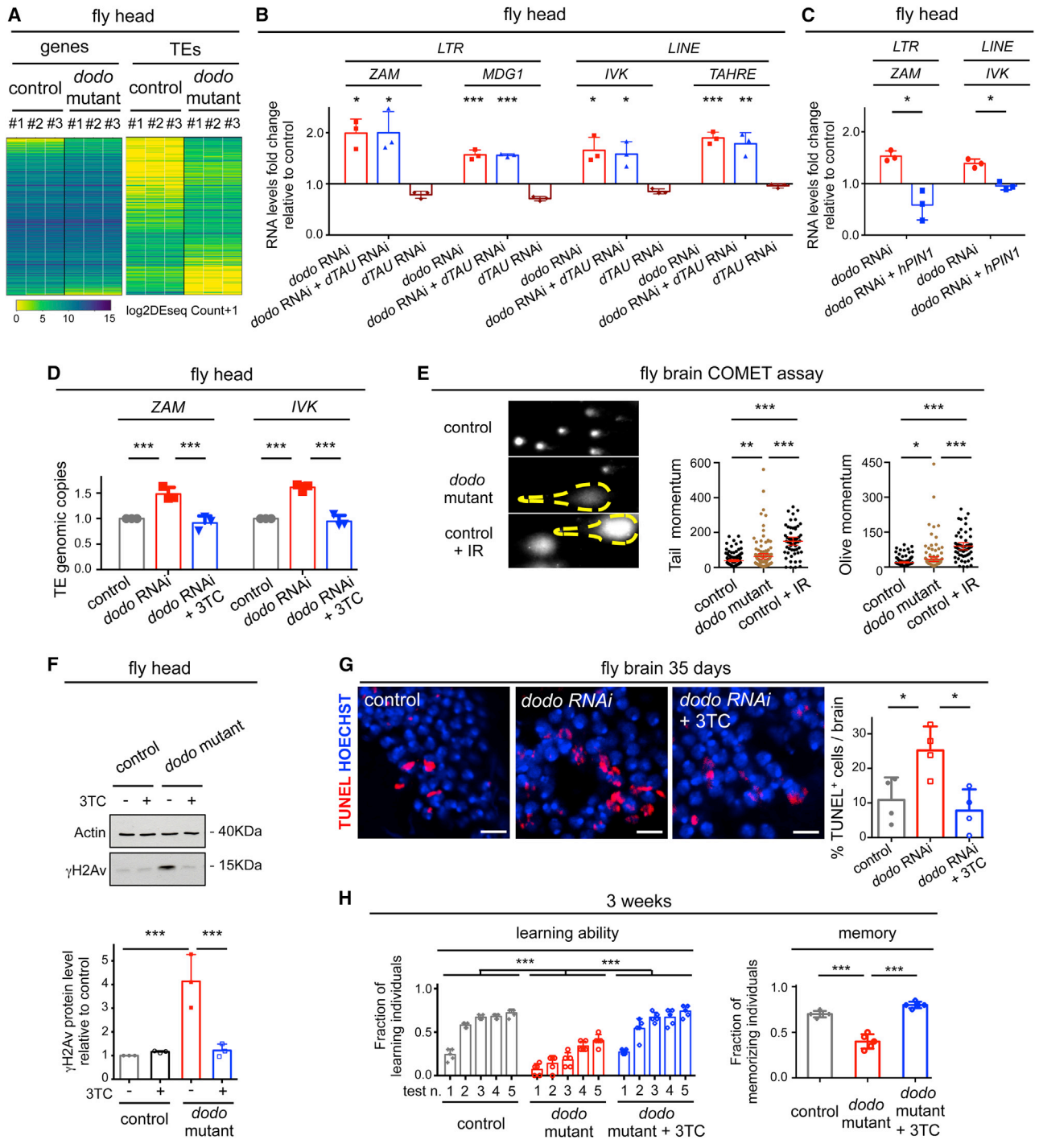

Figure 2. Dodo restrains TE activity in *Drosophila* brains

(A) RNA-seq heatmap (#1–3, triplicates of 4-day-old WT control and *dodo*^{EY03779} mutant flies). TE locus-specific expression was analyzed by SQuIRE (Software for Quantifying Interspersed Repeat Expression). See also Table S1.

(B) qPCR analysis of TE expression in 4-day-old flies expressing *dodo* RNAi (*Elav* > *dodo*^{KK108535}), *dodo* RNAi and *dTAU* RNAi (*Elav* > *dodo*^{KK108535} > *dTau*$^{TRiP.HM05101}$), and *dTAU* RNAi (*Elav* > *dTau*$^{TRiP.HM05101}$) relative to control flies (*UAS-dodo*^{KK108535}).

(C) qPCR analysis of TE expression in 4-day-old flies expressing *dodo* RNAi (*Elav* > *dodo*^{KK108535}) and *dodo* RNAi and *hPIN1* (*Elav* > *dodo*^{KK108535} > *hPIN1*) relative to control flies (*UAS-dodo*^{KK108535}).

(D) qPCR quantification of TE genomic copy number (relative to control), by copy number variation (CNV) assay, in 4 days old wt control, *dodo*^{EY03779} mutant and 100 μM 3TC-fed *dodo*^{EY03779} mutant flies.

(legend continued on next page)

HP1a state (Figure S3A), suggesting that loss of Dodo could lead to derepression of HP1a-targeted HC.

To validate the effect of loss of Dodo on HC, we selected a representative group of HP1a-targeted LTR (*ZAM*) and LINE-like (*IVK* and *TAHRE*) TEs upregulated in the *dodo* mutant and HP1a target genes upregulated strongly (*Toll-9* and *CG33926*, with logarithmic fold change $\log_2$FC > 7) or mildly (*CG40006* and *Nipped-A*, $\log_2$FC = 0.3–0.5) in the *dodo* mutant (Table S1). For these targets, we performed chromatin immunoprecipitation (ChIP)-qPCR for the HP1a-associated repressive mark H3K9me3 and the active transcription mark H3K9ac, in *dodo* mutant and WT fly heads. For all targets, we observed decreased H3K9me3 and increased H3K9ac in the *dodo* mutant (Figures 3A and S3B). H3K9me3 was also reduced in the HP1a-targeted HC region *H23* (Figure 3A), which is deficient in TEs and genes (Salvany et al., 2012), suggesting a broad effect of Dodo loss leading to HC relaxation.

Furthermore, we selected a representative group of PcG target genes strongly upregulated (Ets21C, Fbp1, and CG10814, $\log_2$FC = 2–4) or not differentially expressed (*exex* and *Antp*) in the *dodo* mutant (Table S1). For these targets, we performed ChIP-qPCR for the PcG-associated facultative HC mark H3K27me3 in *dodo* mutant and WT fly heads. We observed decreased H3K27me3 and increased H3K9ac for upregulated genes but no changes for those not differentially expressed (Figure S3B).

These findings suggest that loss of Dodo exerts a broad effect on HC, mainly affecting HP1a-dependent HC.

Next we investigated the mechanisms underlying the association of Dodo and HP1a functions. In the *dodo* mutant brain, HP1a foci were strongly reduced compared with WT flies (Figures 3B and 3C). Furthermore, in the head, neuron-specific $dodo^{RNAi}$ was associated with reduced HP1a protein levels, which were rescued by *hPIN1* expression (Figure 3C). A similar HP1a reduction was observed in *dodo* mutant ovaries (Figure S3C). A decrease in HP1a protein levels in $dodo^{RNAi}$ fly heads also correlated with a strong reduction in H3K9me3 protein levels (Figure 3D), which were rescued by *HP1a* and *hPIN1* overexpression (Figures 3D, S3D, and S3E), demonstrating that Dodo maintained repressive HC through HP1a. This epistatic relationship was further supported by evidence showing that, in $HP1a^{05/+}$ heterozygous mutant brains, HP1a protein level reduction (Figure S3F) did not affect Dodo protein levels and localization (Figures S3G and S3H) while being associated with H3K9me3 reduction (Figure S3I) and increased RNA levels of several of the TEs upregulated by loss of Dodo (Figure S3J).

We then assessed whether Dodo reduction could perturb tissue function through HC relaxation. In aged WT fly brains, HP1a protein levels decreased, and those of γH2Av increased (Figure 3E), alterations that were accelerated in $dodo^{EY03779}$ homozygous but not $dodo^{EY03779/+}$ heterozygous mutants (Figures 3E and 1A), suggesting that drop of Dodo function under a critical threshold unleashes HC relaxation. Furthermore, in the brains of flies expressing neuron-specific $dodo^{RNAi}$, all alterations associated with loss of Dodo (TE derepression, DNA damage, neurodegeneration, and cognitive and motor defects) were suppressed by *HP1a* overexpression (Figures 3F–3J and S3K).

These results demonstrate that, by maintaining HP1a protein levels and HC, Dodo restrains TE activity and preserves tissue function.

Dodo stabilizes HP1a in complex with LamB in a phosphorylation-dependent manner

Loss of Dodo did not alter *HP1a* mRNA levels (Figure S4A) but caused HP1a protein degradation because treating *dodo* mutant or $dodo^{RNAi}$-expressing fly brains with the proteasome inhibitor MG132 restored HP1a protein to levels similar to the WT (Figures S4B and 4A). In human cells, HP1α degradation has been shown to depend on the E3 ubiquitin ligases HECW2, RNF123, and FBXW10 (Chaturvedi and Parnaik, 2010; Chaturvedi et al., 2012; Krishnamoorthy et al., 2018). In WT fly brains, treatment with the PIN1 catalytic inhibitor KPT6566 (Campaner et al., 2017) was associated with reduction of HP1a protein levels, which was rescued by knockout of *Hecw* (Figure 4B), the *Drosophila* ortholog of *HECW2* (Fajner et al., 2021). Furthermore, HP1a was ubiquitinated by Hecw, as shown by *in vitro* assays (Figure S4C), and in the brain, Hecw overexpression reduced HP1a protein levels (Figure S4D).

In human epithelial cell lines, HP1α protein levels are regulated by Lamin A/C, which inhibits HECW2-dependent HP1α degradation (Chaturvedi and Parnaik, 2010; Chaturvedi et al., 2012; Krishnamoorthy et al., 2018). However, fly brain neurons express LamB and much less Lamin C (LamC) (Lenz-Böhme et al., 1997), whose further reduction did not alter HP1a protein levels, as

(E) Alkaline COMET assay in 4-day-old WT control, $dodo^{EY03779}$ mutant, and 5-Gy γ-irradiated (IR) WT fly brains. Quantification shows mean tail and olive momentum values ± SD of grouped n = 20 individuals (n = 60–150 cells/group). ***p < 0.001, **p < 0.01, *p < 0.05 by one-way ANOVA with Tukey correction.
(F) Western blot analysis of γH2Av in 4-day-old WT control and $dodo^{EY03779}$ mutant flies and in 100 μM 3TC-fed, 4-day-old WT control and $dodo^{EY03779}$ mutant flies. Actin was used as reference for quantification, showing mean values ± SD of n = 3 biological replicates. ***p < 0.001 by one-way ANOVA with Tukey correction.
(G) TUNEL in cryosections of control flies (*Elav-GAL4*), flies expressing *dodo* RNAi (*Elav* > $dodo^{KK108535}$), and 100 μM 3TC-fed flies expressing *dodo* RNAi. Nuclei are stained with Hoechst. Quantifications show mean values ± SD of n = 4 individuals (200–400 cells/individual). *p < 0.05 by one-way ANOVA with Tukey correction.
(H) Learning and memory assays in WT control, $dodo^{EY03779}$ mutant, and 100 μM 3TC-fed *dodo* mutant flies. For learning assays, values represent mean ± SD of n = 5 groups (n = 20 individuals/group). For each group, flies positive for phototaxis were iteratively trained five times (test n. 1–5) for the ability to associate light with a negative stimulus (0.1 M quinine solution, bitter taste) that inhibits phototaxis (aversive learning). For each test, the fractions of individuals positive (unlearned) and negative (learning) for phototaxis were calculated. ***p < 0.001 by two-way ANOVA with Tukey correction. For short-term memory assays, values represent mean ± SD of an n = 20 individuals group. Single groups of trained flies were left for 5 h at 25°C and re-tested. The fractions of individuals positive (memory-defective) and negative (memorizing) for phototaxis were calculated. ***p < 0.001 by 001 by one-way ANOVA with Tukey correction.
For qPCR, *rp49* (B and C) and *DMRT1C* (D) were used as references for quantifications, showing mean values ± SD of n = 3 biological replicates. ***p < 0.001, *p < 0.05 by one-way ANOVA with Tukey correction. In (B), p values versus control are reported. Scale bars, 5 μm. See also Figure S2.

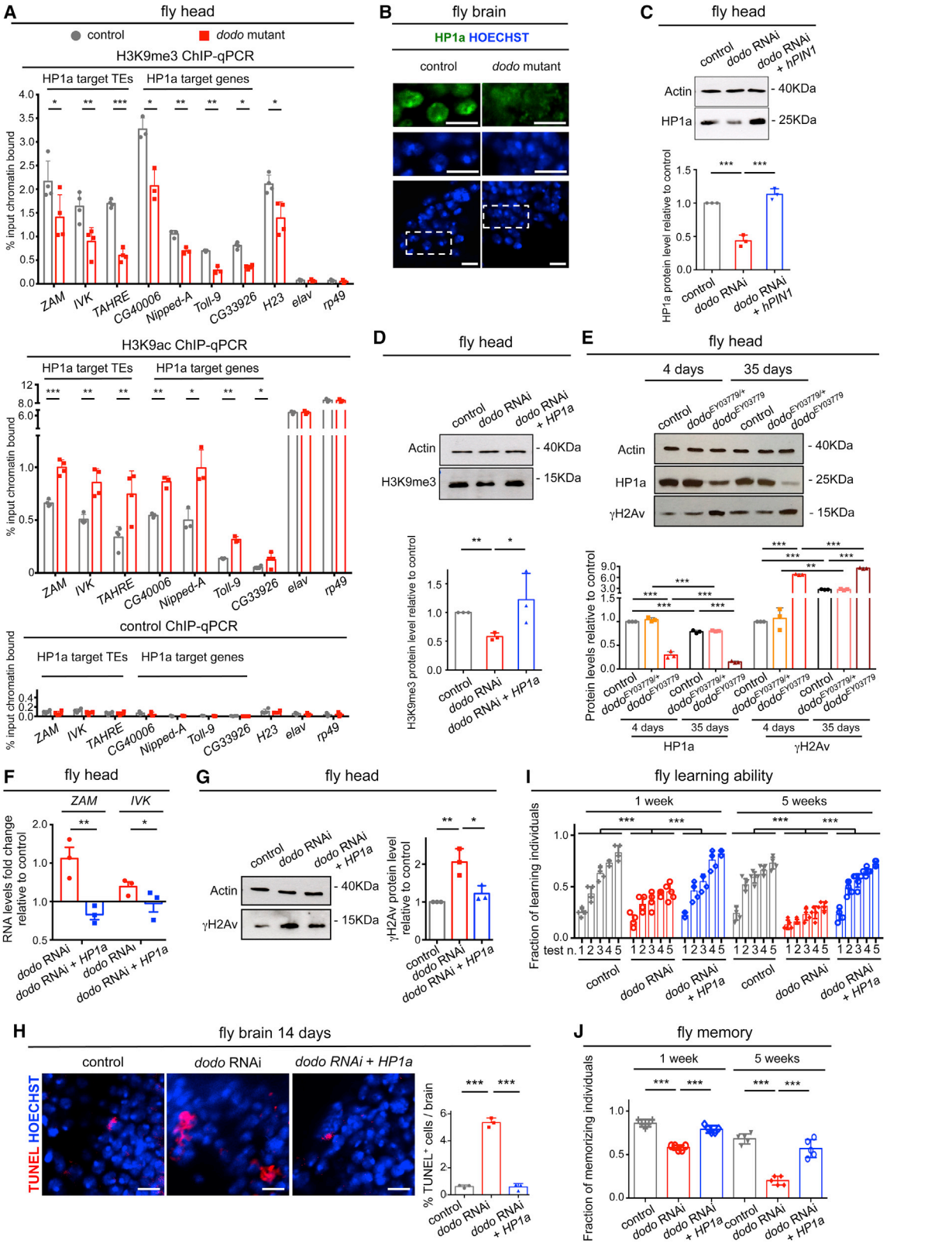

(legend on next page)

shown in $lamC^{CB04957/+}$ and $lamC^{G00158/+}$ mutants (Figure S4E). In contrast, LamB reduction in $lamB^{K2/+}$ and $lamB^{04643/+}$ mutants was associated with decreased HP1a protein levels (Figure S4F), in line with previous reports (Frost et al., 2016), whereas HP1a mRNA and Dodo protein levels were not reduced (Figures S4F and S4G). In $lamB^{K2/+}$ heads, HP1a protein levels were restored by *Hecw* knockout and MG132 treatment (Figures S4H and S4I).

These results indicate that, like Dodo, LamB is required to prevent Hecw-dependent HP1a degradation.

Nuclear Lamin proteins anchor HP1α to the NE (Poleshko et al., 2013; Solovei et al., 2013), stabilize Lamin-interacting proteins (Johnson et al., 2004), and organize LADs (Guelen et al., 2008). HP1α anchoring to type B Lamin has been proposed to involve the LamB receptor (LBR) (Kourmouli et al., 2000; Ye and Worman, 1996; Ye et al., 1997), however LBR^{RNAi} did not alter HP1a protein levels in fly heads (Figure S4J), suggesting that it was not required for LamB-dependent HP1a stability. PIN1/Dodo is a phosphorylation-specific *cis-trans* prolyl isomerase that promotes substrate conformational changes relevant for protein interactions (Liou et al., 2011; Rustighi et al., 2009; Zacchi et al., 2002). Moreover, Dodo is enriched at the NE (Figures S1A and S1B); therefore, we wondered whether it could favor HP1a-stabilizing interaction with LamB. In WT fly heads, HP1a formed a protein complex with LamB, an interaction that was strongly decreased in the *dodo* mutant (Figure 4C), whereas total LamB levels were unaltered (Figure S4K). Similar results were obtained in brains treated with the PIN1 inhibitor KPT6566 (Figure 4D), suggesting that Dodo isomerase activity was required for LamB/HP1a interaction.

Regulation of protein complex formation by PIN1 involves recognition of the pS/T-P motif, and, indeed, LamB/HP1a interaction was phosphorylation dependent because treating WT fly head lysates with λ-phosphatase strongly reduced the amount of LamB co-immunoprecipitating with HP1a (Figure S4L). Inspection of LamB and HP1a amino acid sequences revealed that only the former harbors phosphorylatable S/T-P sites, suggesting that LamB could be the substrate of Dodo. Indeed, in fly brains, Dodo co-immunoprecipitated with (Figure 4E) and bound *in situ* LamB (as shown by proximity ligation assay [PLA]; Figure S4M). In interphase nuclei, LamB phosphorylatable S/T-P sites have been proposed to be targeted by CDK5 (Machowska et al., 2015). To assess whether CDK5 was required for Dodo/LamB protein interaction, we treated WT fly brains with the CDK5 inhibitor roscovitine (Meijer et al., 1997), which strongly decreased the amount of LamB co-immunoprecipitating with Dodo and HP1a (Figures 4F and 4G), and reduced HP1a but not Dodo protein levels (Figure 4H).

These results suggest that Dodo is essential for anchoring HP1a to LamB in a phosphorylation-dependent manner, maintaining HP1a protein stability (Figure 4I).

Dodo protects NE structure and HC under mechanical stress

Lamin proteins are major contributors of NE structure, and their assembly and function are regulated by phosphorylation (Machowska et al., 2015; Milbradt et al., 2016). In fly brains, $lamB^{K2/+}$ mutation was associated with LamB invaginations (Figure S5A), a hallmark of NE structural defects (Frost et al., 2016). This prompted us to assess whether phosphorylation-dependent regulation of LamB by Dodo affected NE structure. In the fly brain, $dodo^{RNAi}$ was associated with LamB invaginations, which were not prevented by *HP1a* overexpression (Figure 5A) nor observed in $HP1a^{05/+}$ mutant flies (Figure S5B), suggesting that they were not linked with HC status. In *dodo* mutant fly brains, NE and chromatin morphometry revealed a statistically significant but modest reduction of nuclear circularity (Figure S5C) without nuclear size change (Figures S5D and S5E) compared with WT flies, suggesting that loss of Dodo affects nuclear deformability.

Figure 3. Dodo restrains TE activity by maintaining HP1a-dependent HC in the *Drosophila* brain

(A) Chromatin immunoprecipitation (ChIP)-qPCR with anti-H3K9me3 and anti-H3K9Ac antibodies or protein A/G-Agarose as a negative control in 4-day-old WT control and $dodo^{EY03779}$ mutant flies. The abundance of each histone mark within the indicated genomic regions was quantified by calculating the percentage of input chromatin bound, by qPCR. Values represent mean ± SD of n = 4 biological replicates. *elav* and *rp49* were used as control genes constitutively expressed in *Drosophila* brain neurons.

(B) Immunofluorescence analysis of HP1a protein in 4-day-old WT control and $dodo^{EY03779}$ mutant brain cryosections.

(C and D) Western blot analysis of HP1a (C) and H3K9me3 (D) in 4-day-old control flies (*UAS-dodo*^{KK108535}) and flies expressing *dodo* RNAi (*Elav* > *dodo*^{KK108535}), *dodo* RNAi and *hPIN1* (*Elav-GAL4* > *dodo*^{KK108535} > *hPIN1*; C), or *dodo* RNAi and *HP1a* (*Elav* > *UAS-dodo*^{KK108535} > *HP1a*; D).

(E) Western blot analysis of HP1a and γH2Av in WT control, $dodo^{EY03779/+}$ heterozygous, and $dodo^{EY03779}$ homozygous flies. The experiment also included analysis of Dodo (Figure 1A).

(F) qPCR analysis of TE expression in 4-day-old flies expressing *dodo* RNAi (*Elav* > *dodo*^{KK108535}) and *dodo* RNAi and *HP1a* (*Elav* > *UAS-dodo*^{KK108535} > *HP1a*) relative to control flies (*UAS-dodo*^{KK108535}).

(G and H) Western blot analysis of γH2Av (G) and TUNEL cryosections (H) in 4-day-old control flies (*UAS-dodo*^{KK108535}) and flies expressing *dodo* RNAi (*Elav* > *dodo*^{KK108535}) or *dodo* RNAi and *HP1a* (*Elav* > *UAS-dodo*^{KK108535} > *HP1a*).

(I and J) Learning (I) and memory (J) assays in control flies (*UAS-dodo*^{KK108535}) and flies expressing *dodo* RNAi (*Elav* > *dodo*^{KK108535}) or *dodo* RNAi and HP1a (*Elav* > *dodo*^{KK108535} > *HP1a*). For learning assays, values represent mean ± SD of n = 5 groups (n = 20 individuals/group). For each group, flies positive for phototaxis were iteratively trained five times (test n. 1–5) for the ability to associate light with a negative stimulus (0.1 M quinine solution, bitter taste) that inhibits phototaxis (aversive learning). For each test, the fractions of individuals positive (unlearned) and negative (learning) for phototaxis were calculated. ***$p < 0.001$ by two-way ANOVA with Tukey correction. For short-term memory assays, values represent mean ± SD of an n = 20 individuals group. Single groups of trained flies were left for 5 h at 25°C and re-tested. The fractions of individuals positive (memory-defective) and negative (memorizing) for phototaxis were calculated. ***$p < 0.001$ by one-way ANOVA with Tukey correction.

For immunofluorescence and TUNEL, nuclei were stained with Hoechst. Actin (western blots) and *rp49* (qPCR) were used as references for quantification, showing mean values ± SD of n = 3 biological replicates. ***$p < 0.001$, **$p < 0.01$, *$p < 0.05$ by two-way (E) and one-way (C, D, and G) ANOVA with Tukey correction and two-tailed paired (A) and unpaired (F) Student's t test. For TUNEL, quantification shows mean values ± SD of n = 4 individuals (200–400 cells/individual). ***$p < 0.001$ by one-way ANOVA with Tukey correction. Scale bars, 5 μm. See also Figure S3.

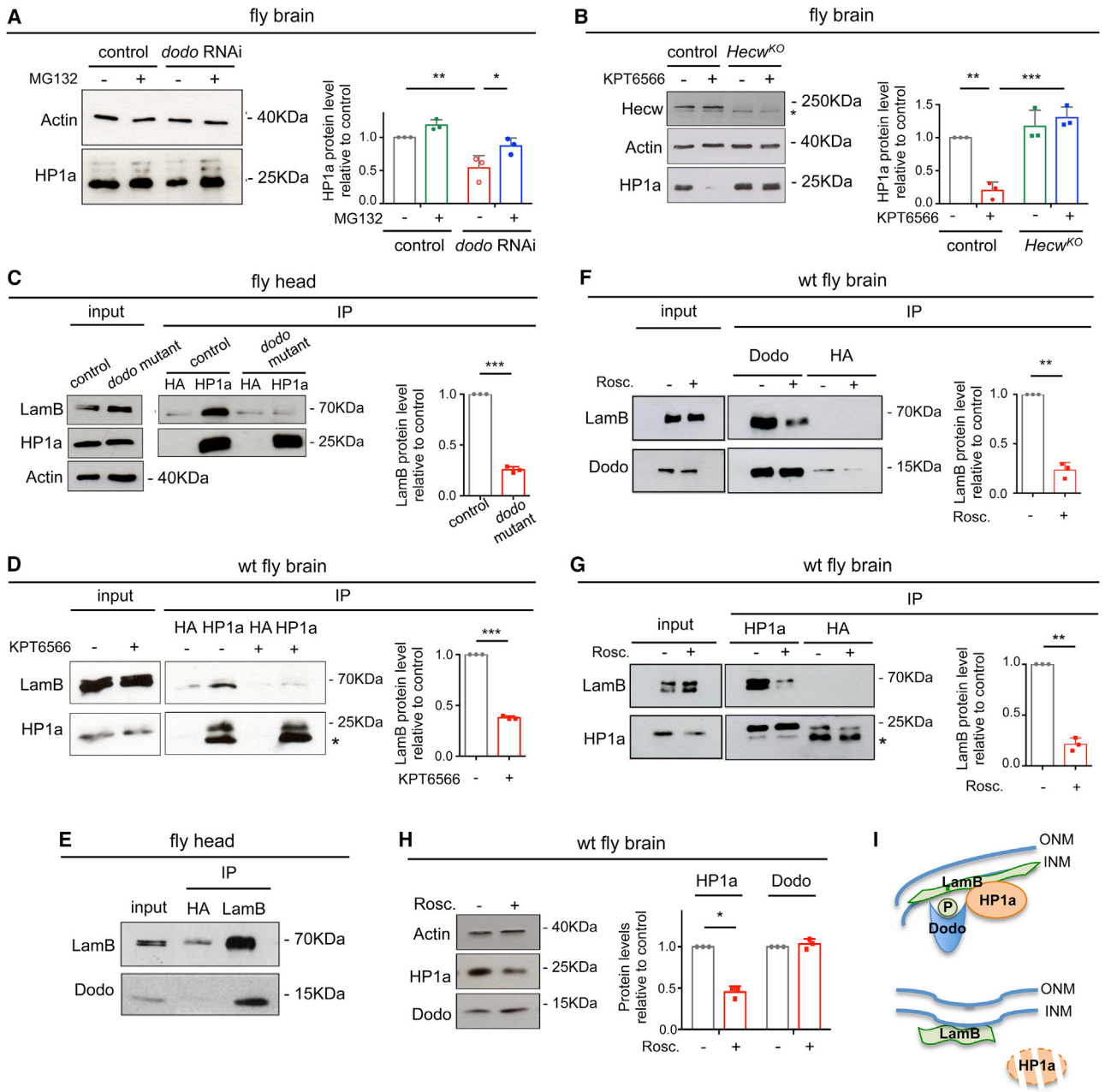

Figure 4. Dodo anchors to LamB and stabilizes HP1a protein in a phosphorylation-dependent manner

(A) Western blot analysis of HP1a in 4-day-old control (*UAS-dodo*^{KK108535}) and *dodo* RNAi-expressing (*Elav- > dodo*^{KK108535}) fly brains treated with DMSO vehicle or 25 μM MG132 (3 h, room temperature). Actin was used as reference for quantification, showing mean values ± SD of n = 3 biological replicates. **p < 0.01, *p < 0.05 by two-way ANOVA with Tukey correction.

(B) Western blot analysis of Hecw and HP1a in 4-day-old WT control and *Hecw*^{KO} fly brains treated with DMSO vehicle or the PIN1 inhibitor KPT6566 (5 μM, 3 h, room temperature). Actin was used as reference for quantification, showing mean values ± SD of n = 3 biological replicates. ***p < 0.001, **p < 0.01 by two-way ANOVA with Tukey correction.

(C) Protein co-immunoprecipitation (coIP) in 4 day-old WT and *dodo*^{EY03779} mutant fly head lysates. WT and *dodo*^{EY03779} samples containing equivalent HP1a amounts were immunoprecipitated with anti-HP1a C1A9 antibody, loaded on polyacrylamide gels, and analyzed by western blot.

(D) Protein coIP in 4-day-old WT fly brains treated (3 h, room temperature) with DMSO or the PIN1 inhibitor KPT6566 (5 μM). Samples containing equivalent HP1a amounts were immunoprecipitated with anti-HP1a C1A9 antibody, loaded on polyacrylamide gels, and analyzed by western blot.

(E) Protein coIP in 4 days old wt fly head.

(F and G) Protein coIP in 4-day-old WT fly brains treated (6 h, room temperature) with DMSO or 50 μM roscovitine (Rosc). Samples containing equivalent Dodo (F) or HP1a (G) amounts were immunoprecipitated with anti-PIN1 and anti-HP1a C1A9 antibodies, loaded on polyacrylamide gels, and analyzed by western blot.

(H) Western blot analysis of HP1a and Dodo in 4-day-old fly brains treated (6 h, room temperature) with DMSO or 50 μM Rosc.

(legend continued on next page)

The Lamin nucleoskeleton, through the LINC protein complex, controls how mechanical stimuli are linked to chromatin regulation (Kirby and Lammerding, 2018). By controlling LamB conformation, Dodo could maintain NE structure and function upon mechanical stress, preventing HC relaxation and gene expression alteration. To test this hypothesis, we used jasplakinolide, a drug that causes mechanical stress through actin hyperpolymerization (Holzinger, 2009). This treatment induced LamB invaginations in *dodo*$^{EY03779/+}$ heterozygous and enhanced LamB invaginations in *dodo*^{EY03779} homozygous mutants but did not alter LamB structure in WT neurons (Figure 5B), correlating with upregulation of HP1a-targeted TE RNA levels (Figure 5C).

Because jasplakinolide also directly affects nuclear actin, which is required for HC dynamics (Mahmood et al., 2020; Xie et al., 2018a, 2018b), we generated a genetic model of mechanical stress based on cytoplasmic F-actin hyperpolymerization by Actin capping protein-b (Cpb) knockdown. In fly brains, neuron-specific *cpb*^{RNAi} caused cytoplasmic F-actin hyperpolymerization (Figure 5D), and, similar to knockout of its ortholog *Capzb* in mice (Pocaterra et al., 2019), was associated with actomyosin hypercontraction, as shown by phosphorylation of Spaghetti squash (Sqh; the ortholog of MLC-2 [myosin light chain-2]) (Figure S5F), leaving Dodo protein levels unaffected (Figure S5G). *cpb*^{RNAi} did not alter HP1a and H3K9me3 levels unless Dodo function was reduced by *dodo*$^{EY03779/+}$ heterozygosity (Figure 5E).

Mechanical stress has been reported to induce CDK5 activity (Gallazzini et al., 2011; Sharma and Sicinski, 2020; Xu et al., 2011), and we observed that, in WT fly brains, treatment with the CDK5 inhibitor roscovitine caused LamB invaginations (Figure 5D) and reduced HP1a protein levels (Figure 5F). Treatment with the PIN1 catalytic inhibitor PIB (Uchida et al., 2003) caused similar LamB defects (Figure S5H). Hence we assessed whether, upon mechanical stress, phosphorylation by CDK5 was required for maintenance of LamB protein structure and function by Dodo. In fly brains, *cpb*^{RNAi} did not cause LamB invaginations (Figure 5D) or reduced HP1a protein levels (Figure 5F) unless LamB phosphorylation was inhibited by roscovitine (Figures 5D and 5F).

Dysfunctional hTAU has been shown to act as a physiopathological mechanical stress, leading to LamB invaginations through LINC complex alteration and HC relaxation and TE upregulation in fly brains (Frost et al., 2014, 2016; Sun et al., 2018). Under these conditions (Figure S6A), Dodo protein levels were strongly reduced (Figure S6B) compared with control flies, and Dodo level restoration (Figure S6B) suppressed all hTAU-dependent alterations; namely, LamB invaginations, HP1a and H3K9me3 protein reduction, TE upregulation, neurodegeneration, and fly motor defects (Figures S6C–S6H).

These results suggest that Dodo regulates LamB structure and function in a phosphorylation-dependent manner, safeguarding NE structure and HC against mechanical stress.

PIN1 impairment is associated with NE dysfunction, TE toxicity, and pro-inflammatory mechanisms in mammals

Recent evidence suggests that NE stress and cytosolic accumulation of reverse-transcribed TEs induce the pro-inflammatory cGAS/STING/IFN (Cyclic GMP-AMP synthase/Stimulator of interferon genes/interferon) pathway and senescence (De Cecco et al., 2019; Earle et al., 2020). We investigated whether PIN1 impairment, causing NE weakening and TE hyperactivity, led to cGAS/STING/IFN induction and neurodegeneration. We treated mouse neocortical primary neurons with PIB and observed nuclear LamB1 invaginations (Figure 6A), HP1α proteasomal degradation (Figure 6B), and H3K9me2 reduction (Figure 6C). This correlated with increased TE RNA levels (Figure 6D), induction of cGAS/STING/IFN transcriptional signature (Figure 6D), and cell death that was suppressed by 3TC (Figure 6E).

Furthermore, adult *Pin1*$^{-/-}$ mouse brain neurons displayed NE structure alterations, as shown by LamB1 and LamC invaginations (Figures 6F, S7A, and S7B); decreased LamB1/HP1α protein interaction, as shown by PLA (Figure 6G); reduced HP1α protein (but not mRNA) levels (Figures 6H, S7C, and S7D); decreased H3K9me2 (Figures 6I, 6J, and S7B); enhanced TE expression (Figure 6K); DNA damage, as shown by γH2AX, pChk1, and 53BP1 staining (Figure 6L); and *IFNB1* RNA induction (Figures 6K and S7E).

These results suggest that PIN1 has a fundamental function, conserved from *Drosophila* to mammals, in maintaining NE structure and HC, preventing TE aberrant mobilization, induction of pro-inflammatory pathways, and loss of homeostasis at the cell and tissue levels.

PIN1 reduction is associated with NE dysfunction and TE deregulation in AD

In several aging-related diseases, including AD, neuroinflammation has been documented by different approaches, including transcriptomics (Blalock et al., 2004, 2011; Humphries et al., 2015; Roy et al., 2020). We investigated whether impairment of PIN1 function in regulation of NE and HC could be associated with AD. A somatic protein-destabilizing *PIN1* mutation has been found in individuals with AD and shown to correlate with brain pathology (Park et al., 2019). We analyzed the affected tissue and observed that PIN1 protein level reduction correlated with LamB1 invaginations and H3K9me2 reduction (Figure 7A).

Furthermore, we assessed whether PIN1 dysfunction and TE upregulation were associated in AD by analyzing PIN1 mRNA levels in available datasets of brains of individuals with AD shown previously to display TE upregulation (Guelen et al., 2008; Sun et al., 2018). In two independent cohorts from the Mayo and Religious Orders Study and Memory and Aging Project (ROSMAP) studies, PIN1 mRNA levels were reduced significantly (Figure 7B) compared with controls. Analysis of PIN1 and TE RNA level correlation in the Mayo study showed that PIN1 expression anti-

(I) Model of phosphorylation- and Dodo-dependent regulation of LamB function in anchoring and maintaining the stability of HP1a protein. The outer nuclear membrane (ONM) and inner nuclear membrane (INM) are indicated.

For coIP, anti-HA antibody was used as negative control, and quantifications show mean values ± SD of n = 3 biological replicates. ***$p < 0.001$, **$p < 0.01$ two-tailed paired (Student's t test). (E) is representative of n = 2 biological replicates. In western blots, bands indicated by asterisks correspond to non-specific signal (B) and the light chains of the antibody used for IP (D and G). See also Figure S4.

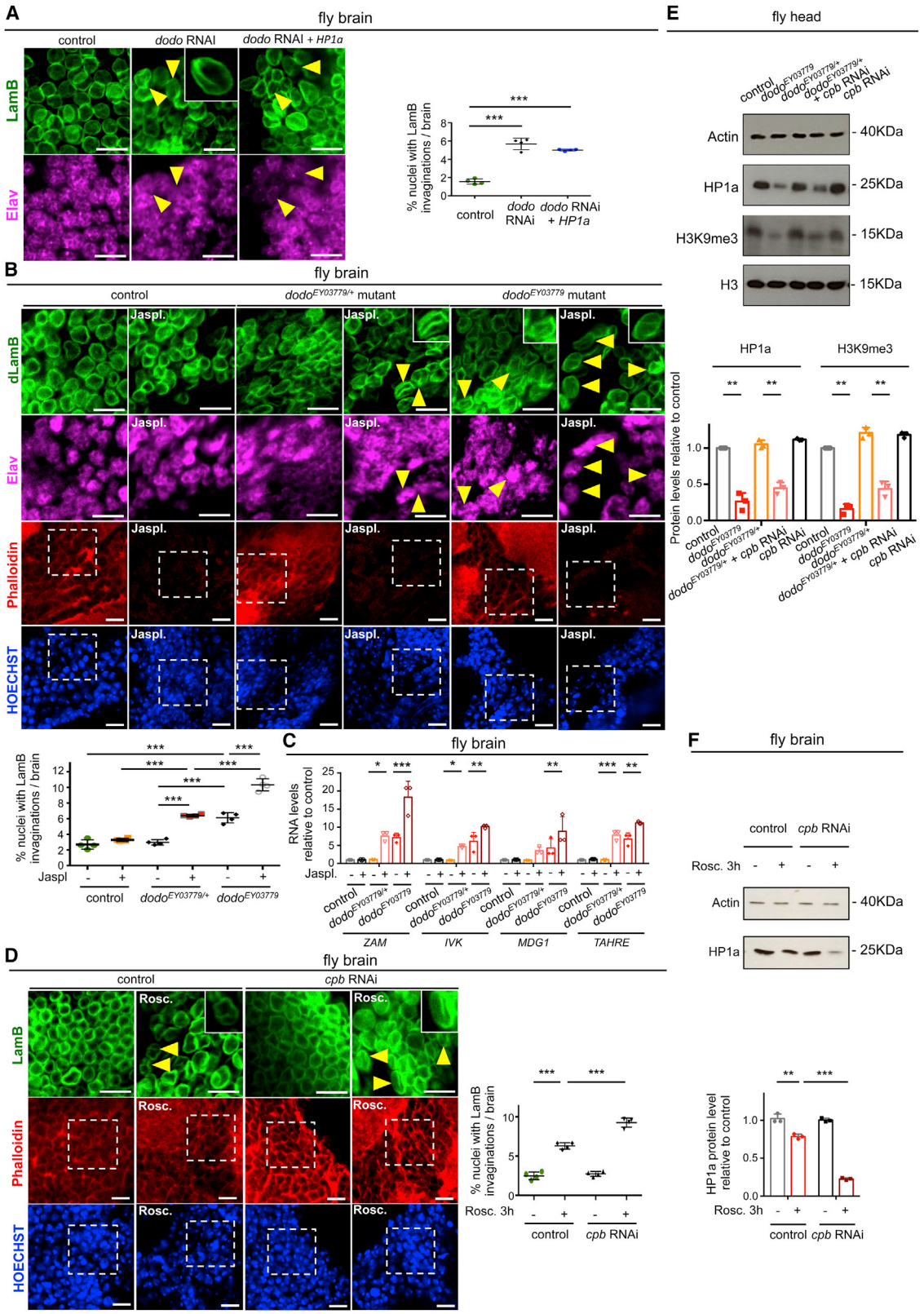

(legend on next page)

correlated with expression of almost all (10 of 12) upregulated TE subfamilies (Figure 7B).

We also evaluated whether AD transcriptome alterations were associated with a gene expression signature linked to PIN1/HP1α impairment. We compiled a list of the human orthologs of HP1a target genes upregulated in *dodo* mutant heads and analyzed their expression in individuals from the Mount Sinai Brain Bank (MSBB) study, stratified according to cognitive impairment and pathology (Braak stage) (Blalock et al., 2004, 2011; Roy et al., 2020). Many genes of this signature displayed increased expression correlating with disease progression (Figure 7C; Table S2).

These results suggest that impairment of PIN1 function in the maintenance of NE structure and HC has an important role in AD.

DISCUSSION

The organization of HP1α-dependent HC has been shown to involve multiple mechanisms, including tethering to NE, protein PTMs, and condensation in liquid droplets by phase separation (Hildebrand and Dekker, 2020; Zhang et al., 2019). NE tethering organizes chromatin in LADs, which are crucial to restrain TE activity and control cell fate and tissue homeostasis (Holla et al., 2020; Vazquez et al., 2019). Our findings that PIN1 maintains LamB structure and function in tethering and stabilization of HP1α suggest that LAD organization and function could depend on PIN1.

Phosphorylation of Lamins has been proposed to regulate their binding to chromatin (Machowska et al., 2015), and changes in response to mechanical stimuli (Buxboim et al., 2014; Nava et al., 2020). The activity of CDK5, which targets Lamins (Machowska et al., 2015), has been shown to be induced by mechanical stress (Gallazzini et al., 2011; Sharma and Sicinski, 2020; Xu et al., 2011). It is conceivable that PIN1, by coupling LamB phosphorylation by CDK5 with HP1α stability, could contribute to adapt LAD organization and gene expression in response to mechanical cues.

Lamin phosphorylation regulates NE assembly during the cell cycle (Machowska et al., 2015), and pathologic alterations of Lamin structure, as in laminopathies and cancer, have been shown to predispose to NE rupture (Denais et al., 2016; Earle et al., 2020). Recently, NE breaches have been shown to trigger specific repair mechanisms involving the inner nuclear membrane proteins LEMD2 and LAP2β and ESCRT-III proteins for maintaining nucleo-cytoplasm compartmentalization and cell survival (Chen et al., 2021; Halfmann et al., 2019; Raab et al., 2016; Young et al., 2020). We observed that, in *Pin1*$^{-/-}$ mouse brain neurons, the structures of LamB1 and LamC were altered, and in *dodo* mutant fly brains, similar LamB alterations were accompanied by transcriptional induction of ESCRT-III components. Therefore, it is conceivable that PIN1 dysfunction could affect NE functionality, causing NE rupture and repair mechanism activation.

Regulation of Lamin protein structure recently emerged as a crucial mechanism to safeguard NE integrity against mechanical stress. Indeed, LamA protein assembly has been shown to increase following actomyosin tension to maintain NE rigidity, preventing nuclear damage (Buxboim et al., 2014; Cho et al., 2019). Moreover, a NE-protective response to mechanical stress has been shown to correlate with Lamin phosphorylation in epithelial cells (Nava et al., 2020). Our results suggest that PIN1 could fine-tune NE deformability to mechanical cues, preserving NE integrity.

NE alterations, leading to HC relaxation and unscheduled TE activity, have important consequences in different pathologies associated with aging and mechanical stress, including AD and cancer (Uhler and Shivashankar, 2017). Interestingly, recent transcriptome analyses showed that PIN1 gene expression declines with age in human brain regions vulnerable to AD (Lanke et al., 2018). These observations, together with our findings that Dodo protein levels decline with age in fly brains and that Dodo loss recapitulates *Pin1*$^{-/-}$ mice premature aging phenotypes, suggest that PIN1, by preserving LamB and HP1α protein function, could promote healthy aging. Furthermore, evidence showing that PIN1 is consistently under-expressed in individuals with AD showing TE upregulation and that a transcriptional signature linked to PIN1/HP1α impairment correlates with AD severity supports the clinical relevance of our findings.

Our results offer opportunities for improving treatments to control the onset or slow down the progression of degenerative diseases associated with HP1α dysfunction and TE hyperactivity, such as AD, by acting at multiple levels: preventing cognitive defects with reverse transcriptase inhibitors, maintaining HP1α protein levels by HECW2 inhibition, and sustaining PIN1 function.

Figure 5. Phosphorylation by CDK5 and Dodo activity protect LamB structure and HC condensation from mechanical stress

(A) Whole-mount immunofluorescence analysis of Lamin B (LamB) protein in 4-day-old control flies (*UAS-dodo*^{KK108535}) and flies expressing *dodo* RNAi (*Elav* > *dodo*^{KK108535}) or *dodo* RNAi and *HP1a* (*Elav* > *dodo*^{KK108535} > *HP1a*). Inset: super-resolution image of LamB invagination.

(B and C) Whole-mount immunofluorescence analysis of LamB protein (B) and qPCR analysis of TE expression (C) in 4-day-old WT control, *dodo*$^{EY03779/+}$ heterozygous, and *dodo*^{EY03779} homozygous fly brains treated (3 h, room temperature) with DMSO vehicle or 1 μM jasplakinolide (Jaspl). The top panels correspond to dashed squares indicated in the bottom panels.

(D) Whole-mount immunofluorescence analysis of LamB protein in 7-day-old control (*UAS-cpb*^{GD9299}) and *cpb* RNAi-expressing (*Elav* > *cpb*^{GD9299}) fly brains treated (3 h, room temperature) with DMSO vehicle or 50 μM Rosc. The top panels correspond to the dashed squares in the center and bottom panels.

(E) Western blot analyses of HP1a and H3K9me3 in 7-day-old control flies (*UAS-cpb*^{GD9299}) and flies expressing *cpb* RNAi (*Elav* > *cpb*^{GD9299}), *dodo*^{EY03779} homozygous, *dodo*$^{EY03779/+}$ heterozygous, and *cpb* RNAi-expressing *dodo*$^{EY03779/+}$ heterozygous (*dodo*$^{EY03779/+}$ + *cpb* RNAi).

(F) Western blot analyses of HP1a in 7-day-old control (*UAS-cpb*^{GD9299}) and *cpb* RNAi-expressing (*Elav* > *cpb*^{GD9299}) fly brains treated (3 h, room temperature) with DMSO vehicle or 50 μM Rosc.

For immunofluorescence, neurons are stained with anti-Elav antibody, F-Actin with Phalloidin, and nuclei with Hoechst. Quantifications of nuclei with LamB invaginations (arrowheads) show mean values ± SD of n = 4 individuals (200–400 cells/individual). Actin (western blots) and *actin* (qPCR) were used as references for quantifications, which show mean values ± SD of n = 3 biological replicates. ***p < 0.001, **p < 0.01, *p < 0.05 by one-way (A) or two-way (B–F) ANOVA with Tukey correction. Scale bars, 5 μm. See also Figures S5 and S6.

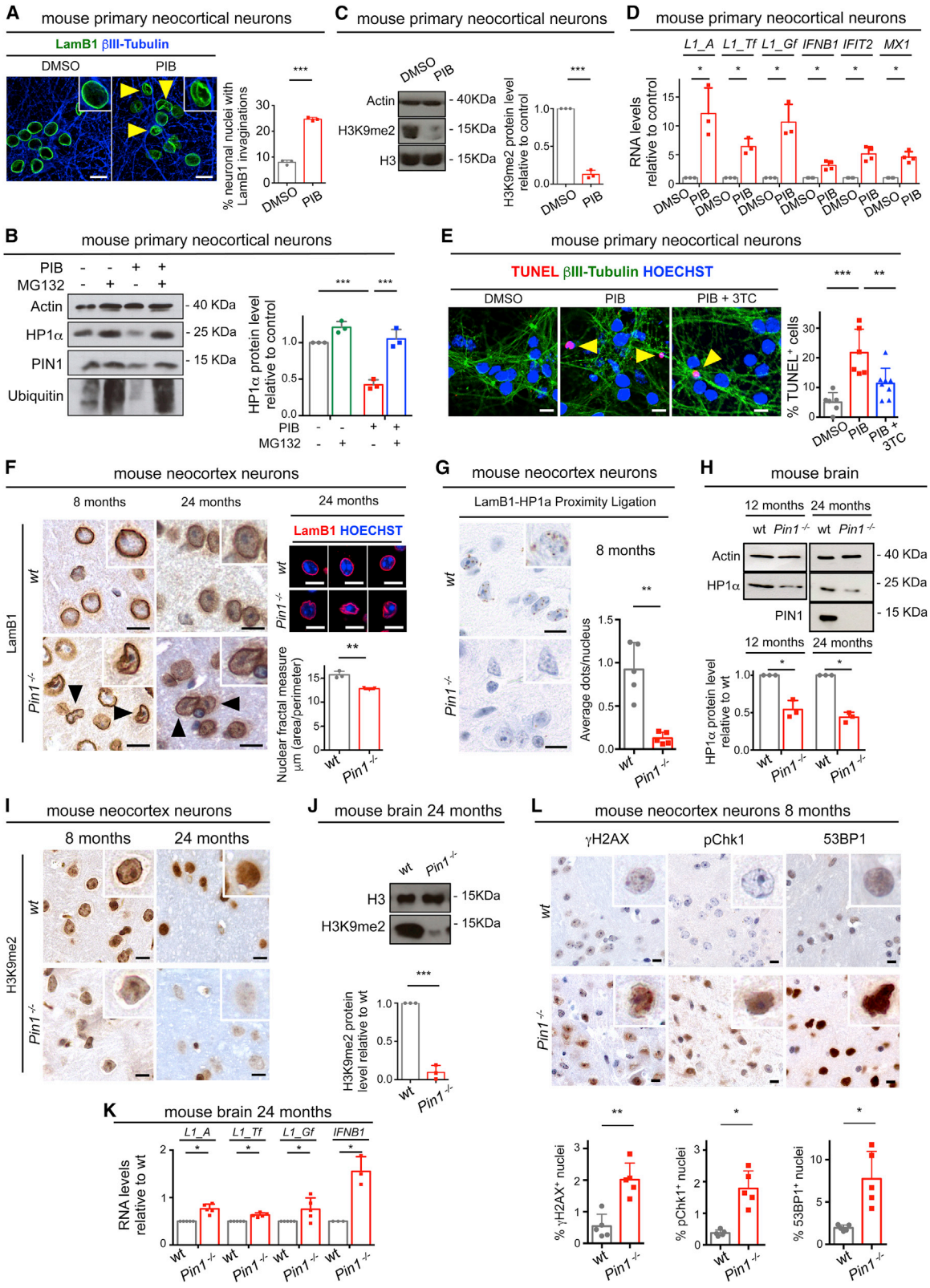

(legend on next page)

STAR★METHODS

Detailed methods are provided in the online version of this paper and include the following:

- KEY RESOURCES TABLE
- RESOURCE AVAILABILITY
  - Lead contact
  - Materials availability
  - Data and code availability
- EXPERIMENTAL MODEL AND SUBJECT DETAILS
  - Fly stocks and treatments
  - Primary cultures
  - Mice
  - Human brain tissues
- METHOD DETAILS
  - *Drosophila* organ dissection
  - *Drosophila* ex-vivo brain culture
  - *Drosophila* organ whole mount TUNEL
  - *Drosophila* organ whole mount immunofluorescence
  - *Drosophila* tissue cryosections
  - *Drosophila* tissue cryosection TUNEL
  - *Drosophila* tissue cryosection immunofluorescence
  - Proximity ligation assay (PLA) in *Drosophila* tissue
  - COMET assay in *Drosophila* tissue
  - *Drosophila* photoreceptor live imaging
  - Fly negative geotaxis assay
  - Fly fertility assay
  - Fly learning and memory assays
  - Immunohistochemistry of analysis of mouse and human tissue sections
  - Immunofluorescence analysis of mouse and human tissue sections and mouse primary neuronal cultures
  - Proximity ligation assay (PLA) assay in mouse tissue
  - Image acquisition and analysis
  - Total RNA and genomic DNA purification
  - Paired end sequencing of *Drosophila* head RNA and analyses
  - Analysis of TE loci and gene chromatin states in mature neurons
  - PIN1/HP1α signature and human sample dataset analysis
  - PIN1 expression quantification in AD transcriptomic datasets
  - Correlation between PIN1 and TEs expression in AD transcriptomic datasets
  - cDNA synthesis
  - Chromatin IP from *Drosophila* tissues
  - Real time quantitative PCR
  - Protein IP
  - Protein purification
  - Western blot
  - *In vitro* assays
  - Oligonucleotides used in this study
- QUANTIFICATION AND STATISTICAL ANALYSIS

SUPPLEMENTAL INFORMATION

Supplemental information can be found online at https://doi.org/10.1016/j.celrep.2021.109694.

ACKNOWLEDGMENTS

We thank M. Foiani, G.V. Shivashankar, P. Maiuri, F. Ferrari, Y.C. Liou, and A. Testa for discussions; G. Pastore, the Trieste University microscopy facility, D. Parazzoli, A. Oldani, and E. Martini (Imaging Unit, IFOM, Milan) for technical support; E. Buratti and C. Stuani (ICGEB Trieste) for access to Bioruptor; the Developmental Studies Hybridoma Bank (DSHB), Vienna *Drosophila* Resource Center (VDRC), Bloomington Drosophila Stock Center (BDSC), RIKEN BioResource Research Center, S.C.R. Elgin (Washington University, St. Louis, USA), S. Piccolo (University of Padova), B. Mollereau (École Normale Supérieure de Lyon, France), E.Y. Kim (Ajou University, Republic of Korea), W.X. Li (University of Rochester, USA), D. Andrenacci (National Research Council, Bologna, Italy), P. Dourlen (University of Lille, France), and R.E. Ward (University of Kansas, USA) for reagents and fly stocks; and O.J. Marshall (University of Tasmania, Australia) for assistance with access to public databases. The G.D.S. lab is supported by grants from the Cariplo Foundation (2014-0812), the Italian University and Research Ministry (PRIN-2017HWTP2K_004 and MIUR-ARS01_00876), Associazione Italiana per la Ricerca sul Cancro (AIRC) Special Program 5x1000 (22759), AIRC-IG (22174), INTERREG V-A Italia-Austria P-CARE (ITAT1050), and Ministero della Salute (RF-2019-12368718). This work was also supported by FFABR 2017 and FIRB n. RBFR10V8K6 grants from the Italian Ministry of University and Research (to V.S.) and EU FP7/AIRC Reintegration (iCARE 17885) and Trieste University FRA 2018 grants (to F.N.). E.C. and A.B. were supported by Fondazione Veronesi post-doctoral fellowships. The F.d.d.F. lab is supported by an ERC advanced grant (TELORNAGING 835103), AIRC-IG (21762), Telethon (GGP17111), AIRC 5x1000 (21091), ERC PoC

Figure 6. Impairment of PIN1/HP1α is associated with IFN induction in mice

(A–E) Immunofluorescence analysis of Lamin B1 (LamB1) protein (A), western blot analyses of HP1α (B) and H3K9me2 (C), qPCR analysis of TE expression (D), and TUNEL (E) in mouse primary neurons treated with DMSO vehicle, 5 μM PIB (48+48 h double hit), 1 μM MG132 (16 h, B) and 100 μM 3TC (48 h, E). In (A), neurons are marked by anti-βIII-tubulin antibody, and quantification of LamB1 invaginated nuclei (arrowheads) shows mean values ± SD of n = 3 biological replicates (400–700 cells/condition), with ***$p < 0.001$ by two-tailed unpaired Student's t test. In (E), arrowheads indicate TUNEL-positive nuclei. Nuclei are stained with Hoechst. Quantification shows mean values ± SD of 5–8 fields (50–100 cells/field), with *$p < 0.05$ by one-way ANOVA with Tukey correction.

(F–L) Immunohistochemistry analyses of LamB1 (F, left panels); H3K9me2 (I); γH2AX, pChk1, and 53BP1 (L) proteins; LamB1-HP1α proximity ligation assay (PLA; G); immunofluorescence analysis of LamB1 protein (F, right panels), western blot analyses of HP1α and PIN1 (H) and H3K9me2 (J); and qPCR analysis of TE expression (K) in *Pin1*$^{-/-}$ mice and WT littermates. In (F), arrowheads indicate LamB1 invaginated nuclei (left panels, inset). Nuclei are stained with Hoechst (right panels). For quantification of LamB1 deformation, the nuclear fractal measure was computed as the ratio between area and perimeter (circularity) of each structure, showing mean values ± SD of n = 3 individuals (5 fields/individual), with **$p < 0.05$ by two-tailed unpaired Student's t test. In (G) and (L), quantifications show mean values ± SD of 5 fields/individual (n = 1 WT and n = 2 *Pin1*$^{-/-}$ individuals), with ***$p < 0.01$, **$p < 0.05$ by two-tailed unpaired Student's t test.

Actin (western blot) and *GAPDH* (qPCR) were used as references for quantifications, which show mean values ± SD of n = 3 biological replicates (B–D) or individuals (H, J, and K), with ***$p < 0.001$, *$p < 0.05$ by two-way ANOVA with Tukey correction (B) and two-tailed unpaired Student's t test (C, D, H, J, and K). Scale bars, 15 μm. See also Figure S7.

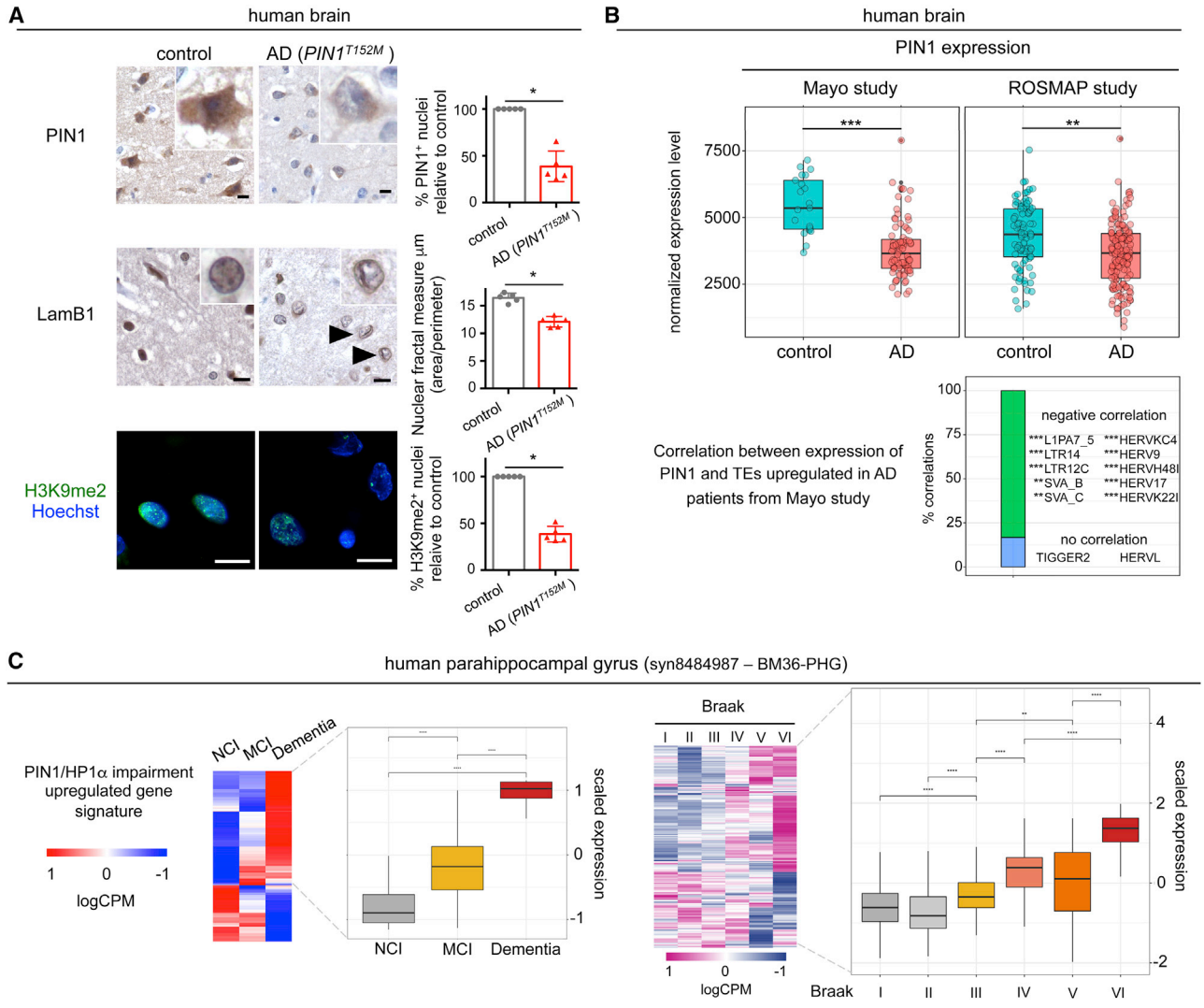

Figure 7. Impairment of PIN1/HP1α is associated with AD progression

(A) Immunohistochemistry analyses of PIN1 (top panels) and LamB1 (center panels) and immunofluorescence analysis of H3K9me2 (bottom panels) proteins in non-demented control individuals and an individual with Alzheimer's disease (AD) harboring the somatic $PIN1^{T152M}$ mutation. Arrowheads indicate LamB1 invaginated nuclei (inset). For quantification of LamB1 deformation, the nuclear fractal dimension measure was computed as the ratio between area and perimeter (circularity) of each structure. Quantifications show mean values ± SD of 5 fields/individual (n = 2 non-demented controls and n = 1 AD individual). *p < 0.05 by two-tailed unpaired Student's t test.

(B) Top panels: analysis of PIN1 RNA expression (normalized counts as calculated by default DESeq2 median of ratios) in non-demented control individuals and individuals with AD in the Mayo (20 controls and 80 AD individuals) and ROSMAP (87 controls and 157 AD individuals) study datasets. False discovery rate (FDR) indicates Benjamini-Hochberg-corrected ***p < 0.001 and **p < 0.01, calculated by the DESeq2 Wald test. Bottom panel: analysis of correlation between the expression levels of PIN1 and the n = 12 TEs upregulated in individuals with AD versus controls in the Mayo study dataset (FDR < 0.05).

(C) Left panels: group-averaged RNA expression heatmap of 207 (of 310) and average scaled expression of 141 (of 207) human orthologs of HP1a target genes repressed by Dodo in the *Drosophila* brain (Table S1) in the parahippocampal gyrus (BM36-PHG) of individuals with no (NCI controls, clinical dementia rating [CDR] = 0, n = 26) or mild (MCI, CDR = 0.5, n = 27) cognitive impairment and dementia (AD, CDR > 1, n = 106). Right panels: group-averaged expression heatmap of 207 (of 310) and average scaled expression of 141 (of 207) human orthologs of HP1a target genes repressed by Dodo in the *Drosophila* brain (Table S1) in the parahippocampal gyrus (BM36-PHG) of Braak I (n = 20), II (n = 33), III (n = 32), IV (n = 20), V (n = 19), and VI (n = 43) individuals. ****p < 0.0001, ***p < 0.001, **p < 0.01, by two-tailed unpaired Student's t test. See also Table S2.

(FIREQUENCER 875139), PRIN 2017 "RNA and Genome Instability", AriSLA 2021 "DDR&ALS", POR FESR 2014–2020 Regione Lombardia (InterSLA project), FRRB (Fondazione Regionale per la Ricerca Biomedica) under the frame of the European Joint Program (EJP RD COFUND-EJP 825575) on Rare Diseases with funding from the European Union Horizon 2020 research and innovation program. The results published here include analyses of data that were collected thanks to NIA grants P50 AG016574, R01 AG032990, U01 AG046139, R01 AG018023, U01 AG006576, U01 AG006786, R01 AG025711,

R01 AG017216, R01 AG003949 to the Mayo Clinic, and R01AG15819 (ROSMAP, genomics and RNA-seq).

AUTHOR CONTRIBUTIONS

F.N. conceived and designed experiments, performed *Drosophila* experiments and bioinformatic analyses, analyzed data, supervised the work, prepared figures, and wrote the paper. G.F.B. designed and performed *Drosophila* and mouse experiments and analyzed data. I.A.P.V. performed *Drosophila* and mouse experiments. A.S., L.C., and C.D. performed *Drosophila* experiments. A.B., E.V., A.R., and E.C. performed mouse experiments. M. Santorsola, F.A., and R.S. performed bioinformatics analyses. V.F. and E.M. performed ubiquitination and RFP::Hecw experiments and provided reagents and fly stocks. V.C. and C.T. performed immunohistochemistry and immunofluorescence on mouse and human sections. C.F.V. performed nuclear morphometric analyses in mammalian tissues. M. Santo and O.B.A. performed primary neuron experiments. S.F. designed CNV assays. U.G. provided expertise and performed COMET assays. F.d.d.F. provided expertise and helped with manuscript editing. S.P. supervised ubiquitination and RFP::Hecw experiments and provided feedback. A.M. supervised primary neuron experiments and provided feedback. S.G. provided expertise and feedback. F.M. conceived and designed experiments, analyzed data, and supervised the work. V.S. conceived the study and designed and performed *Drosophila* experiments. G.D.S. conceived the study, supervised the project, and wrote the manuscript.

DECLARATION OF INTERESTS

The authors declare no competing interests.

Received: February 16, 2021
Revised: June 29, 2021
Accepted: August 19, 2021
Published: September 14, 2021

REFERENCES

Allshire, R.C., and Madhani, H.D. (2018a). Ten principles of heterochromatin formation and function. Nat. Rev. Mol. Cell Biol. *19*, 229–244.

Andrews, S. (2015). FASTQC: A Quality Control tool for High Throughput Sequence Data (Babraham Bioinformatics).

Ansaloni, F., Scarpato, M., Di Schiavi, E., Gustincich, S., and Sanges, R. (2019). Exploratory analysis of transposable elements expression in the C. elegans early embryo. BMC Bioinformatics *20* (*Suppl 9*), 484.

Atchison, F.W., Capel, B., and Means, A.R. (2003). Pin1 regulates the timing of mammalian primordial germ cell proliferation. Development *130*, 3579–3586.

Bao, W., Kojima, K.K., and Kohany, O. (2015). Repbase Update, a database of repetitive elements in eukaryotic genomes. Mob. DNA *6*, 11.

Bertolio, R., Napoletano, F., Mano, M., Maurer-Stroh, S., Fantuz, M., Zannini, A., Bicciato, S., Sorrentino, G., and Del Sal, G. (2019). Sterol regulatory element binding protein 1 couples mechanical cues and lipid metabolism. Nat. Commun. *10*, 1326.

Blalock, E.M., Geddes, J.W., Chen, K.C., Porter, N.M., Markesbery, W.R., and Landfield, P.W. (2004). Incipient Alzheimer's disease: microarray correlation analyses reveal major transcriptional and tumor suppressor responses. Proc. Natl. Acad. Sci. USA *101*, 2173–2178.

Blalock, E.M., Buechel, H.M., Popovic, J., Geddes, J.W., and Landfield, P.W. (2011). Microarray analyses of laser-captured hippocampus reveal distinct gray and white matter signatures associated with incipient Alzheimer's disease. J. Chem. Neuroanat. *42*, 118–126.

Bolger, A.M., Lohse, M., and Usadel, B. (2014). Trimmomatic: a flexible trimmer for Illumina sequence data. Bioinformatics *30*, 2114–2120.

Buxboim, A., Swift, J., Irianto, J., Spinler, K.R., Dingal, P.C.D.P., Athirasala, A., Kao, Y.R.C., Cho, S., Harada, T., Shin, J.W., and Discher, D.E. (2014). Matrix elasticity regulates lamin-A,C phosphorylation and turnover with feedback to actomyosin. Curr. Biol. *24*, 1909–1917.

Chaturvedi, P., and Parnaik, V.K. (2010). Lamin A rod domain mutants target heterochromatin protein 1α and β for proteasomal degradation by activation of F-box protein, FBXW10. PLoS ONE *5*, e10620.

Campaner, E., Rustighi, A., Zannini, A., Cristiani, A., Piazza, S., Ciani, Y., Kalid, O., Golan, G., Baloglu, E., Shacham, S., et al. (2017). A covalent PIN1 inhibitor selectively targets cancer cells by a dual mechanism of action. Nat. Commun. *8*, 15772.

Chaturvedi, P., Khanna, R., and Parnaik, V.K. (2012). Ubiquitin ligase RNF123 mediates degradation of heterochromatin protein 1α and β in lamin A/C knockdown cells. PLoS ONE *7*, e47558.

Chen, N.Y., Kim, P.H., Tu, Y., Yang, Y., Heizer, P.J., Young, S.G., and Fong, L.G. (2021). Increased expression of LAP2β eliminates nuclear membrane ruptures in nuclear lamin-deficient neurons and fibroblasts. Proc. Natl. Acad. Sci. USA *118*, e2107770118.

Cho, S., Vashisth, M., Abbas, A., Majkut, S., Vogel, K., Xia, Y., Ivanovska, I.L., Irianto, J., Tewari, M., Zhu, K., et al. (2019). Mechanosensing by the Lamina Protects against Nuclear Rupture, DNA Damage, and Cell-Cycle Arrest. Dev. Cell *49*, 920–935.e5.

De Cecco, M., Ito, T., Petrashen, A.P., Elias, A.E., Skvir, N.J., Criscione, S.W., Caligiana, A., Brocculi, G., Adney, E.M., Boeke, J.D., et al. (2019). L1 drives IFN in senescent cells and promotes age-associated inflammation. Nature *566*, 73–78.

Denais, C.M., Gilbert, R.M., Isermann, P., McGregor, A.L., Te Lindert, M., Weigelin, B., Davidson, P.M., Friedl, P., Wolf, K., and Lammerding, J. (2016). Nuclear envelope rupture and repair during cancer cell migration. Science *352*, 353–358.

Dobin, A., Davis, C.A., Schlesinger, F., Drenkow, J., Zaleski, C., Jha, S., Batut, P., Chaisson, M., and Gingeras, T.R. (2013). STAR: ultrafast universal RNA-seq aligner. Bioinformatics *29*, 15–21.

Earle, A.J., Kirby, T.J., Fedorchak, G.R., Isermann, P., Patel, J., Iruvanti, S., Moore, S.A., Bonne, G., Wallrath, L.L., and Lammerding, J. (2020). Mutant lamins cause nuclear envelope rupture and DNA damage in skeletal muscle cells. Nat. Mater. *19*, 464–473.

Fajner, V., Giavazzi, F., Sala, S., Oldani, A., Martini, E., Napoletano, F., Parazzoli, D., Cerbino, R., Maspero, E., Vaccari, T., et al. (2021). The ubiquitin ligase Hecw controls oogenesis and neuronal homeostasis by promoting the liquid state of ribonucleoprotein particles. bioRxiv. https://doi.org/10.1101/2020.05.30.124933.

Frost, B., Hemberg, M., Lewis, J., and Feany, M.B. (2014). Tau promotes neurodegeneration through global chromatin relaxation. Nat. Neurosci. *17*, 357–366.

Frost, B., Bardai, F.H., and Feany, M.B. (2016). Lamin Dysfunction Mediates Neurodegeneration in Tauopathies. Curr. Biol. *26*, 129–136.

Gallazzini, M., Heussler, G.E., Kunin, M., Izumi, Y., Burg, M.B., and Ferraris, J.D. (2011). High NaCl-induced activation of CDK5 increases phosphorylation of the osmoprotective transcription factor TonEBP/OREBP at threonine 135, which contributes to its rapid nuclear localization. Mol. Biol. Cell *22*, 703–714.

Girardini, J.E., Napoli, M., Piazza, S., Rustighi, A., Marotta, C., Radaelli, E., Capaci, V., Jordan, L., Quinlan, P., Thompson, A., et al. (2011). A Pin1/mutant p53 axis promotes aggressiveness in breast cancer. Cancer Cell *20*, 79–91.

Girardini, J.E., Walerych, D., and Del Sal, G. (2014). Cooperation of p53 mutations with other oncogenic alterations in cancer. Subcell. Biochem. *85*, 41–70.

Guastella, D., and Valenti, C. (2016). Cartoon filter via adaptive abstraction. J. Vis. Commun. Image Represent. *36*, 149–158.

Guelen, L., Pagie, L., Brasset, E., Meuleman, W., Faza, M.B., Talhout, W., Eussen, B.H., de Klein, A., Wessels, L., de Laat, W., and van Steensel, B. (2008). Domain organization of human chromosomes revealed by mapping of nuclear lamina interactions. Nature *453*, 948–951.

Guo, C., Jeong, H.H., Hsieh, Y.C., Klein, H.U., Bennett, D.A., De Jager, P.L., Liu, Z., and Shulman, J.M. (2018). Tau Activates Transposable Elements in Alzheimer's Disease. Cell Rep *23*, 2874–2880.

Gyori, B.M., Venkatachalam, G., Thiagarajan, P.S., Hsu, D., and Clement, M.V. (2014). OpenComet: an automated tool for comet assay image analysis. Redox Biol. *2*, 457–465.

Halfmann, C.T., Sears, R.M., Katiyar, A., Busselman, B.W., Aman, L.K., Zhang, Q., O'Bryan, C.S., Angelini, T.E., Lele, T.P., and Roux, K.J. (2019). Repair of nuclear ruptures requires barrier-to-autointegration factor. J. Cell Biol. *218*, 2136–2149.

Hildebrand, E.M., and Dekker, J. (2020). Mechanisms and Functions of Chromosome Compartmentalization. Trends Biochem. Sci. *45*, 385–396.

Holla, S., Dhakshnamoorthy, J., Folco, H.D., Balachandran, V., Xiao, H., Sun, L.L., Wheeler, D., Zofall, M., and Grewal, S.I.S. (2020). Positioning Heterochromatin at the Nuclear Periphery Suppresses Histone Turnover to Promote Epigenetic Inheritance. Cell *180*, 150–164.e15.

Holzinger, A. (2009). Jasplakinolide: an actin-specific reagent that promotes actin polymerization. Methods Mol. Biol. *586*, 71–87.

Hu, Y., Flockhart, I., Vinayagam, A., Bergwitz, C., Berger, B., Perrimon, N., and Mohr, S.E. (2011). An integrative approach to ortholog prediction for disease-focused and other functional studies. BMC Bioinformatics *12*, 357.

Huang, W., Sherman, B.T., and Lempicki, R.A. (2009). Systematic and integrative analysis of large gene lists using DAVID bioinformatics resources. Nat. Protoc. *4*, 44–57.

Humphries, C.E., Kohli, M.A., Nathanson, L., Whitehead, P., Beecham, G., Martin, E., Mash, D.C., Pericak-Vance, M.A., and Gilbert, J. (2015). Integrated whole transcriptome and DNA methylation analysis identifies gene networks specific to late-onset Alzheimer's disease. J. Alzheimers Dis. *44*, 977–987.

James, T.C., and Elgin, S.C. (1986). Identification of a nonhistone chromosomal protein associated with heterochromatin in Drosophila melanogaster and its gene. Mol. Cell. Biol. *6*, 3862–3872.

Johnson, B.R., Nitta, R.T., Frock, R.L., Mounkes, L., Barbie, D.A., Stewart, C.L., Harlow, E., and Kennedy, B.K. (2004). A-type lamins regulate retinoblastoma protein function by promoting subnuclear localization and preventing proteasomal degradation. Proc. Natl. Acad. Sci. USA *101*, 9677–9682.

Kaneko, H., Dridi, S., Tarallo, V., Gelfand, B.D., Fowler, B.J., Karikó, K., Yoo, J.W., Lee, D., and Hadziahmetovic, M. (2011). DICER1 deficit induces alu rna toxicity *471*, 325–330.

Kang, S.W., Lee, E., Cho, E., Seo, J.H., Ko, H.W., and Kim, E.Y. (2015). Drosophila peptidyl-prolyl isomerase Pin1 modulates circadian rhythms via regulating levels of PERIOD. Biochem. Biophys. Res. Commun. *463*, 235–240.

Kidiyoor, G.R., Li, Q., Bastianello, G., Bruhn, C., Giovannetti, I., Mohamood, A., Beznoussenko, G.V., Mironov, A., Raab, M., Piel, M., et al. (2020). ATR is essential for preservation of cell mechanics and nuclear integrity during interstitial migration. Nat. Commun. *11*, 4828.

Kirby, T.J., and Lammerding, J. (2018). Emerging views of the nucleus as a cellular mechanosensor. Nat. Cell Biol. *20*, 373–381.

Kourmouli, N., Theodoropoulos, P.A., Dialynas, G., Bakou, A., Politou, A.S., Cowell, I.G., Singh, P.B., and Georgatos, S.D. (2000). Dynamic associations of heterochromatin protein 1 with the nuclear envelope. EMBO J. *19*, 6558–6568.

Krishnamoorthy, V., Khanna, R., and Parnaik, V.K. (2018). E3 ubiquitin ligase HECW2 mediates the proteasomal degradation of HP1 isoforms. Biochem. Biophys. Res. Commun. *503*, 2478–2484.

Kumar, A., Mazzanti, M., Mistrik, M., Kosar, M., Beznoussenko, G.V., Mironov, A.A., Garrè, M., Parazzoli, D., Shivashankar, G.V., Scita, G., et al. (2014). ATR mediates a checkpoint at the nuclear envelope in response to mechanical stress. Cell *158*, 633–646.

Lanke, V., Moolamalla, S.T.R., Roy, D., and Vinod, P.K. (2018). Integrative analysis of hippocampus gene expression profiles identifies network alterations in aging and Alzheimer's disease. Front. Aging Neurosci. *10*, 153.

Larson, K., Yan, S.J., Tsurumi, A., Liu, J., Zhou, J., Gaur, K., Guo, D., Eickbush, T.H., and Li, W.X. (2012). Heterochromatin formation promotes longevity and represses ribosomal RNA synthesis. PLoS Genet. *8*, e1002473.

Lenz-Böhme, B., Wismar, J., Fuchs, S., Reifegerste, R., Buchner, E., Betz, H., and Schmitt, B. (1997). Insertional mutation of the Drosophila nuclear lamin Dm0 gene results in defective nuclear envelopes, clustering of nuclear pore complexes, and accumulation of annulate lamellae. J. Cell Biol. *137*, 1001–1016.

Li, H., Handsaker, B., Wysoker, A., Fennell, T., Ruan, J., Homer, N., Marth, G., Abecasis, G., and Durbin, R.; 1000 Genome Project Data Processing Subgroup (2009). The Sequence Alignment/Map format and SAMtools. Bioinformatics *25*, 2078–2079.

Li, W., Prazak, L., Chatterjee, N., Grüninger, S., Krug, L., Theodorou, D., and Dubnau, J. (2013). Activation of transposable elements during aging and neuronal decline in Drosophila. Nat. Neurosci. *16*, 529–531.

Liou, Y.C., Ryo, A., Huang, H.K., Lu, P.J., Bronson, R., Fujimori, F., Uchida, T., Hunter, T., and Lu, K.P. (2002). Loss of Pin1 function in the mouse causes phenotypes resembling cyclin D1-null phenotypes. Proc. Natl. Acad. Sci. USA *99*, 1335–1340.

Liou, Y.C., Sun, A., Ryo, A., Zhou, X.Z., Yu, Z.X., Huang, H.K., Uchida, T., Bronson, R., Bing, G., Li, X., et al. (2003). Role of the prolyl isomerase Pin1 in protecting against age-dependent neurodegeneration. Nature *424*, 556–561.

Liou, Y.C., Zhou, X.Z., and Lu, K.P. (2011). Prolyl isomerase Pin1 as a molecular switch to determine the fate of phosphoproteins. Trends Biochem. Sci. *36*, 501–514.

Love, M.I., Huber, W., and Anders, S. (2014). Moderated estimation of fold change and dispersion for RNA-seq data with DESeq2. Genome Biol. *15*, 550.

Lu, P.J., Wulf, G., Zhou, X.Z., Davies, P., and Lu, K.P. (1999). The prolyl isomerase Pin1 restores the function of Alzheimer-associated phosphorylated tau protein. Nature *399*, 784–788.

Machowska, M., Piekarowicz, K., and Rzepecki, R. (2015). Regulation of lamin properties and functions: does phosphorylation do it all? Open Biol. *5*, 150094.

Mahmood, S.R., Xie, X., El Said, N.H., Gunsalus, K.C., and Percipalle, P. (2020). β-actin dependent chromatin remodeling mediates compartment level changes in 3D genome architecture. bioRxiv. https://doi.org/10.1101/2020.06.14.150425.

Marshall, O.J., and Brand, A.H. (2017). Chromatin state changes during neural development revealed by in vivo cell-type specific profiling. Nat. Commun. *8*, 2271.

Maspero, E., and Polo, S. (2016). In vitro ubiquitination: Self-ubiquitination, chain formation, and substrate ubiquitination assays. Methods Mol. Biol. *1449*, 153–160.

McCullers, T.J., and Steiniger, M. (2017). Transposable elements in *Drosophila*. Mob. Genet. Elements *7*, 1–18.

Meijer, L., Borgne, A., Mulner, O., Chong, J.P.J., Blow, J.J., Inagaki, N., Inagaki, M., Delcros, J.G., and Moulinoux, J.P. (1997). Biochemical and cellular effects of roscovitine, a potent and selective inhibitor of the cyclin-dependent kinases cdc2, cdk2 and cdk5. Eur. J. Biochem. *243*, 527–536.

MICCAI (2018). Medical image computing and computer assisted intervention – MICCAI 2018. In Proceedings of the 21st International Conference, A.F. Frangi, J.A. Schnabel, C. Davatzikos, C. Alberola-López, and G. Fichtinger, eds..

Milbradt, J., Hutterer, C., Bahsi, H., Wagner, S., Sonntag, E., Horn, A.H.C., Kaufer, B.B., Mori, Y., Sticht, H., Fossen, T., and Marschall, M. (2016). The Prolyl Isomerase Pin1 Promotes the Herpesvirus-Induced Phosphorylation-Dependent Disassembly of the Nuclear Lamina Required for Nucleocytoplasmic Egress. PLoS Pathog. *12*, e1005825.

Napoletano, F., Occhi, S., Calamita, P., Volpi, V., Blanc, E., Charroux, B., Royet, J., and Fanto, M. (2011). Polyglutamine Atrophin provokes neurodegeneration in Drosophila by repressing fat. EMBO J. *30*, 945–958. https://doi.org/10.1038/emboj.2011.1.

Napoletano, F., Gibert, B., Yacobi-Sharon, K., Vincent, S., Favrot, C., Mehlen, P., Girard, V., Teil, M., Chatelain, G., Walter, L., et al. (2017). p53-dependent programmed necrosis controls germ cell homeostasis during spermatogenesis. PLoS Genet. *13*, e1007024.

Nava, M.M., Miroshnikova, Y.A., Biggs, L.C., Whitefield, D.B., Metge, F., Boucas, J., Vihinen, H., Jokitalo, E., Li, X., García Arcos, J.M., et al. (2020).

Heterochromatin-Driven Nuclear Softening Protects the Genome against Mechanical Stress-Induced Damage. Cell *181*, 800–817.e22.

Park, J.S., Lee, J., Jung, E.S., Kim, M.-H., Kim, I.B., Son, H., Kim, S., Kim, S., Park, Y.M., Mook-Jung, I., et al. (2019). Brain somatic mutations observed in Alzheimer's disease associated with aging and dysregulation of tau phosphorylation. Nat. Commun. *10*, 3090.

Pastorino, L., Sun, A., Lu, P.J., Xiao, Z.Z., Balastik, M., Finn, G., Wulf, G., Lim, J., Li, S.H., Li, X., et al. (2006). The prolyl isomerase Pin1 regulates amyloid precursor protein processing and amyloid-β production. Nature *440*, 528–534.

Payer, L.M., and Burns, K.H. (2019). Transposable elements in human genetic disease. Nat. Rev. Genet. *20*, 760–772.

Pindyurin, A.V., Ilyin, A.A., Ivankin, A.V., Tselebrovsky, M.V., Nenasheva, V.V., Mikhaleva, E.A., Pagie, L., van Steensel, B., and Shevelyov, Y.Y. (2018). The large fraction of heterochromatin in Drosophila neurons is bound by both B-type lamin and HP1a. Epigenetics Chromatin *11*, 65.

Pocaterra, A., Santinon, G., Romani, P., Brian, I., Dimitracopoulos, A., Ghisleni, A., Carnicer-Lombarte, A., Forcato, M., Braghetta, P., Montagner, M., et al. (2019). F-actin dynamics regulates mammalian organ growth and cell fate maintenance. J. Hepatol. *71*, 130–142.

Poleshko, A., Mansfield, K.M., Burlingame, C.C., Andrake, M.D., Shah, N.R., and Katz, R.A. (2013). The human protein PRR14 tethers heterochromatin to the nuclear lamina during interphase and mitotic exit. Cell Rep. *5*, 292–301.

Quinlan, A.R., and Hall, I.M. (2010). BEDTools: a flexible suite of utilities for comparing genomic features. Bioinformatics *26*, 841–842.

Raab, M., Gentili, M., De Belly, H., Thiam, H.R., Vargas, P., Jimenez, A.J., Lautenschlaeger, F., Voituriez, R., Lennon-Duménil, A.M., Manel, N., et al. (2016). ESCRT III repairs nuclear envelope ruptures during cell migration to limit DNA damage and cell death. Science *352*, 359–362.

Robin, M., Issa, A.R., Santos, C.C., Napoletano, F., Petitgas, C., Chatelain, G., Ruby, M., Walter, L., Birman, S., Domingos, P.M., et al. (2019). Drosophila p53 integrates the antagonism between autophagy and apoptosis in response to stress. Autophagy *15*, 771–784.

Roy, E.R., Wang, B., Wan, Y.W., Chiu, G., Cole, A., Yin, Z., Propson, N.E., Xu, Y., Jankowsky, J.L., Liu, Z., et al. (2020). Type I interferon response drives neuroinflammation and synapse loss in Alzheimer disease. J. Clin. Invest. *130*, 1912–1930.

Rustighi, A., Tiberi, L., Soldano, A., Napoli, M., Nuciforo, P., Rosato, A., Kaplan, F., Capobianco, A., Pece, S., Di Fiore, P.P., and Del Sal, G. (2009). The prolyl-isomerase Pin1 is a Notch1 target that enhances Notch1 activation in cancer. Nat. Cell Biol. *11*, 133–142.

Rustighi, A., Zannini, A., Tiberi, L., Sommaggio, R., Piazza, S., Sorrentino, G., Nuzzo, S., Tuscano, A., Eterno, V., Benvenuti, F., et al. (2014). Prolyl-isomerase Pin1 controls normal and cancer stem cells of the breast. EMBO Mol. Med. *6*, 99–119.

Salvany, L., Requena, D., and Azpiazu, N. (2012). Functional association between eyegone and HP1a mediates wingless transcriptional repression during development. Mol. Cell. Biol. *32*, 2407–2415.

Seugnet, L., Suzuki, Y., Stidd, R., and Shaw, P.J. (2009). Aversive phototaxic suppression: evaluation of a short-term memory assay in Drosophila melanogaster. Genes Brain Behav. *8*, 377–389.

Sharma, S., and Sicinski, P. (2020). A kinase of many talents: non-neuronal functions of CDK5 in development and disease. Open Biol. *10*, 190287.

Solovei, I., Wang, A.S., Thanisch, K., Schmidt, C.S., Krebs, S., Zwerger, M., Cohen, T.V., Devys, D., Foisner, R., Peichl, L., et al. (2013). LBR and lamin A/C sequentially tether peripheral heterochromatin and inversely regulate differentiation. Cell *152*, 584–598.

Specchia, V., Piacentini, L., Tritto, P., Fanti, L., D'Alessandro, R., Palumbo, G., Pimpinelli, S., and Bozzetti, M.P. (2010). Hsp90 prevents phenotypic variation by suppressing the mutagenic activity of transposons. Nature *463*, 662–665.

Sun, W., Samimi, H., Gamez, M., Zare, H., and Frost, B. (2018). Pathogenic tau-induced piRNA depletion promotes neuronal death through transposable element dysregulation in neurodegenerative tauopathies. Nat. Neurosci. *21*, 1038–1048.

Uchida, T., Takamiya, M., Takahashi, M., Miyashita, H., Ikeda, H., Terada, T., Matsuo, Y., Shirouzu, M., Yokoyama, S., Fujimori, F., and Hunter, T. (2003). Pin1 and Par14 peptidyl prolyl isomerase inhibitors block cell proliferation. Chem. Biol. *10*, 15–24.

Uhler, C., and Shivashankar, G.V. (2017). Regulation of genome organization and gene expression by nuclear mechanotransduction. Nat. Rev. Mol. Cell Biol. *18*, 717–727.

Van Den Brink, D.M., Cubizolle, A., Chatelain, G., Davoust, N., Girard, V., Johansen, S., Napoletano, F., Dourlen, P., Guillou, L., Angebault-Prouteau, C., et al. (2018). Physiological and pathological roles of FATP-mediated lipid droplets in Drosophila and mice retina. PLoS Genet. *14*, e1007627.

Vazquez, B.N., Thackray, J.K., Simonet, N.G., Chahar, S., Kane-Goldsmith, N., Newkirk, S.J., Lee, S., Xing, J., Verzi, M.P., An, W., et al. (2019). SIRT7 mediates L1 elements transcriptional repression and their association with the nuclear lamina. Nucleic Acids Res. *47*, 7870–7885. https://doi.org/10.1093/nar/gkz519.

Xie, X., Almuzzaini, B., Drou, N., Kremb, S., Yousif, A., Farrants, A.Ö., Gunsalus, K., and Percipalle, P. (2018a). β-Actin-dependent global chromatin organization and gene expression programs control cellular identity. FASEB J. *32*, 1296–1314.

Xie, X., Jankauskas, R., Mazari, A.M.A., Drou, N., and Percipalle, P. (2018b). β-actin regulates a heterochromatin landscape essential for optimal induction of neuronal programs during direct reprograming. PLoS Genet. *14*, e1007846.

Xu, J., Tsutsumi, K., Tokuraku, K., Estes, K.A., Hisanaga, S., and Ikezu, T. (2011). Actin interaction and regulation of cyclin-dependent kinase 5/p35 complex activity. J. Neurochem. *116*, 192–204.

Yang, W.R., Ardeljan, D., Pacyna, C.N., Payer, L.M., and Burns, K.H. (2019). SQuIRE reveals locus-specific regulation of interspersed repeat expression. Nucleic Acids Res. *47*, e27.

Ye, Q., and Worman, H.J. (1996). Interaction between an integral protein of the nuclear envelope inner membrane and human chromodomain proteins homologous to Drosophila HP1. J. Biol. Chem. *271*, 14653–14656.

Ye, Q., Callebaut, I., Pezhman, A., Courvalin, J.C., and Worman, H.J. (1997). Domain-specific interactions of human HP1-type chromodomain proteins and inner nuclear membrane protein LBR. J. Biol. Chem. *272*, 14983–14989.

Young, A.M., Gunn, A.L., and Hatch, E.M. (2020). BAF facilitates interphase nuclear membrane repair through recruitment of nuclear transmembrane proteins. Mol. Biol. Cell *31*, 1551–1560.

Zacchi, P., Gostissa, M., Uchida, T., Salvagno, C., Avolio, F., Volinia, S., Ronai, Z., Blandino, G., Schneider, C., and Del Sal, G. (2002). The prolyl isomerase Pin1 reveals a mechanism to control p53 functions after genotoxic insults. Nature *419*, 853–857.

Zamudio, N., and Bourc'his, D. (2010). Transposable elements in the mammalian germline: a comfortable niche or a deadly trap? Heredity *105*, 92–104.

Zannini, A., Rustighi, A., Campaner, E., and Del Sal, G. (2019). Oncogenic Hijacking of the PIN1 Signaling Network. Front. Oncol. *9*, 94.

Zerbino, D.R., Achuthan, P., Akanni, W., Amode, M.R., Barrell, D., Bhai, J., Billis, K., Cummins, C., Gall, A., Girón, C.G., et al. (2018). Ensembl 2018. Nucleic Acids Res. *46* (*D1*), D754–D761.

Zhang, L., and Ward, R.E., 4th. (2011). Distinct tissue distributions and subcellular localizations of differently phosphorylated forms of the myosin regulatory light chain in Drosophila. Gene Expr. Patterns *11*, 93–104.

Zhang, Y.J., Guo, L., Gonzales, P.K., Gendron, T.F., Wu, Y., Jansen-West, K., O'Raw, A.D., Pickles, S.R., Prudencio, M., Carlomagno, Y., et al. (2019). Heterochromatin anomalies and double-stranded RNA accumulation underlie C9orf72 poly(PR) toxicity. Science *363*, eaav2606.

Zhang, W., Qu, J., Liu, G.H., and Belmonte, J.C.I. (2020). The ageing epigenome and its rejuvenation. Nat. Rev. Mol. Cell Biol. *21*, 137–150.

Zhou, X.Z., and Lu, K.P. (2016). The isomerase PIN1 controls numerous cancer-driving pathways and is a unique drug target. Nat. Rev. Cancer *16*, 463–478.

STAR★METHODS

KEY RESOURCES TABLE

REAGENT or RESOURCE	SOURCE	IDENTIFIER
Antibodies		
Rabbit anti-hPIN1/Dodo	G. Del Sal lab (Zacchi et al., 2002)	N/A
Mouse anti-HP1a C1A9	DSHB	Cat#C1A9; RRID: AB_528276
Rabbit anti-HP1a W11	S.C.R. Elgin	N/A
Mouse anti-HA 12CA5	Boehringer Mannheim	N/A
Mouse anti-LamB	DSHB	Cat#ADL67.10; RRID: AB_528336
Mouse anti-LamC	DSHB	Cat# lc28.26; RRID: AB_528339
Mouse anti-γH2Av	DSHB	Cat#UNC93-5.2.1; RRID:AB_2618077
Rat anti-Elav	DSHB	Cat#7E8A10; RRID: AB_528218
Mouse anti-Hecw	S. Polo lab (Fajner et al., 2021)	N/A
Rabbit anti-Actin	Sigma-Aldrich	Cat#A2066; RRID: AB_476693
Rabbit anti-H3K9me3	Diagenode	Cat#C15410056
Guinea pig anti-Sqh1P	R.E. Ward (Zhang and Ward, 2011)	N/A
Rabbit anti-LamB1	Abcam	Cat#ab16048; RRID: AB_443298
Mouse anti-LamB1	Abcam	Cat#ab8982; RRID: AB_1640627
Mouse anti-LamA/C	Santa Cruz	Cat#sc-7292; RRID: AB_627875
Mouse anti-HP1α	Millipore	Cat#05-689; RRID: AB_11213599
Rabbit anti- HP1α	Abcam	Cat#ab109028; RRID: AB_10858495
Mouse anti-Ubiquitin ZTA10	S. Polo lab	N/A
Rabbit anti-Histone H3	Abcam	Cat#ab1791; RRID: AB_302613
Rabbit anti-H3K27me3	Diagenode	Cat#C15410195, RRID: AB_2753161
Rabbit anti-H3K9ac	Millipore	Cat#07-352; RRID: AB_310544
Goat anti-LamA/C	Santa Cruz	Cat#sc-6215; RRID: AB_648152
Rabbit anti-TAU	Gene Tex	Cat#GTX112981
Rabbit anti-γH2AX	Abcam	Cat#ab11174; RRID: AB_297813
Rabbit anti-pChk1	Abcam	Cat#ab58567; RRID: AB_10563825
Rabbit anti-53BP1	Novus	Cat#NB100-304; RRID: AB_10003037
Mouse anti-H3K9me2	Abcam	Cat#ab1220; RRID: AB_449854
Mouse anti-Lamin B1 Clone G-1	Santa Cruz	Cat#sc-373918; RRID: AB_10945297
Rabbit anti-HP1α, Clone EPR5777	Abcam	Cat#ab109028. RRID: AB_10858495
Mouse anti-βIII-Tubulin	N/A	N/A
Goat anti-mouse Alexa Fluor 488	Life Technologies	Cat#A-11001; RRID: AB_2534069
Goat anti-mouse Alexa fluor 568	Life Technologies	Cat#A-11004; RRID: AB_2534072
Donkey anti-mouse Alexa fluor 647	Life Technologies	Cat# A-31571; RRID:AB_162542
Goat anti-rabbit Alexa Fluor 488	Life Technologies	Cat#A-11008; RRID:AB_143165
Goat anti-rabbit Alexa Fluor 568	Life Technologies	Cat#A-11011; RRID: AB_143157
Chicken anti-rabbit Alexa fluor 647	Life Technologies	Cat#A-21443; RRID: AB_2535861
Goat anti-rat Alexa fluor 647	Life Technologies	Cat#A-21247; RRID: AB_141778
Goat anti-guinea pig 568	Life Technologies	Cat#A-11075; RRID: AB_2534119
Goat anti-mouse HRP	Bethyl	Cat#A90-516P; RRID:AB_10631212
Goat anti-rabbit HRP	Bethyl	Cat#A120-201P; RRID:AB_67265
Donkey anti-goat HRP	Bethyl	Cat#A50-201P; RRID: AB_66756
Donkey anti-rabbit IgG	Novex by Life Technologie	N/A
Rabbit anti-mouse IgG	Sigma-Aldrich	N/A

(*Continued on next page*)

Continued

REAGENT or RESOURCE	SOURCE	IDENTIFIER
Bacterial and virus strains		
Rosetta cells	Novagen	N/A
BL21 cells	S. Polo lab	N/A
Biological samples		
Enthorinal cortex samples of non-demented control	Netherlands Brain Bank	#1997-143
Enthorinal cortex samples of non-demented control	Netherlands Brain Bank	#2007-046
Enthorinal cortex samples of AD patient	Netherlands Brain Bank	#2009-040
Chemicals, peptides, and recombinant proteins		
Lamivudine	Sigma-Aldrich	L1295; CAS: 134678-17-4
DMSO	Sigma-Aldrich	D4540; CAS: 67-68-5
PiB	Calbiochem	529627; CAS: 64005-90-9
MG132	Sigma-Aldrich	474790; CAS: 133407-82-6
KPT6566	G. Del Sal Lab	N/A
Roscovitine	Sigma-Aldrich	R7772; CAS: 186692-46-6
Jasplakinolide	Santa Cruz	sc-202191; CAS: 102396-24-7
Insulin	Sigma-Aldrich	I2643; CAS: 11061-68-0
Paraformaldehyde	Sigma-Aldrich	158127; CAS 30525-89-4
HOECHST 33342	Sigma-Aldrich	B2261; CAS: 875756-97-1
Formaldehyde	Sigma-Aldrich	47608; CAS: 50-00-0
Protease inhibitor cocktail	Sigma-Aldrich	P8340
PMSF	Sigma-Aldrich	78830; CAS: 329-98-6
Na3VO4	Sigma-Aldrich	S6508; CAS: 13721-39-6
NaF	Sigma-Aldrich	S7920; CAS: 7681-49-4
Proteinase K	Life Technologies	Cat#25530049
DNase-free RNase	Sigma-Aldrich	Cat#556746
GST- Hecw WT	S. Polo lab	N/A
GST- Hecw C1394W	S. Polo lab	N/A
Lambda Protein Phosphatase	Sigma-Aldrich	Cat#P9614; CAS: 401941-75-1
Critical commercial assays		
In situ cell death detection kit, TMR red (TUNEL)	Sigma-Aldrich	Cat#12156792910
Comet assay kit	Trevigen	Cat#4250-050-K
QuantiTect Reverse Transcription kit	QIAGEN	Cat#205313
Duolink *in situ* Red Starter Kit Mouse/Rabbit (PLA kit)	Sigma Aldrich	Cat# DUO92101
iTaq Universal SYBR Green Supermix	BIO-RAD	Cat#1725125
iQ Multiplex Powermix	BIO-RAD	Cat#172-5849
Deposited data		
w^{1118} and $dodo^{EY03779}$ Drosophila head RNaseq RAW DATA	This paper	European nucleotide archive (ENA): PRJEB41707, https://www.ebi.ac.uk/ena/browser/home
RepBase TE sequences	Bao et al., 2015	https://www.girinst.org/repbase/
Ensembl transcript sequences	Zerbino et al., 2018	http://www.ensembl.org//useast.ensembl.org/index.html?redirectsrc=//www.ensembl.org%2Findex.html
BM36-PHG dataset, The Mount Sinai Brain Bank (MSBB) study	AMP-AD portal; https://adknowledgeportal.synapse.org	Synapse ID: syn8484987; https://www.synapse.org/#!Synapse:syn8484987

(*Continued on next page*)

Continued

REAGENT or RESOURCE	SOURCE	IDENTIFIER
The Religious Orders Study and Memory and Aging Project (ROSMAP) study	AMP-AD portal; https://adknowledgeportal.synapse.org (Guo et al., 2018)	Synapse ID: Synapse:syn3388564; https://www.synapse.org/#!Synapse:syn3388564
The Mayo Clinic Brain Bank (MCBB) study	AMP-AD portal; https://adknowledgeportal.synapse.org (Sun et al., 2018)	Synapse ID: syn23568549; https://www.synapse.org/#!Synapse:syn23568549
Drosophila melanogaster reference genome (BDGP6.22)	Zerbino et al., 2018	http://www.ensembl.org//useast.ensembl.org/index.html?redirectsrc=//www.ensembl.org%2Findex.html
Experimental models: Organisms/strains		
D. melanogaster: w^{1118}	V. Specchia, University of Salento	N/A
D. melanogaster: dodo^{EY03779} y[1] w[67c23] P{y[+mDint2] w[+mC] = EPgy2}dod[EY03779]	Bloomington Drosophila Stock Center	BDSC: 15677 Flybase: FBti0027250
D. melanogaster: UAS-dodo	Kang et al., 2015	Flybase: FBtp0113078
D. melanogaster: UAS-dodo^{KK108535} P{KK108535}VIE-260B	Vienna Drosophila Resource Center	VDRC: 110593 Flybase: FBtp0067021
D. melanogaster: UAS-Luciferase^{RNAi}	Bloomington Drosophila Stock Center	BDSC: 35788
y[1] v[1]; P{y[+t7.7] v[+t1.8] = UAS-LUC. VALIUM10}attP2		Flybase: FBtp0067882
D. melanogaster: lamB^{K2}	D. Andrenacci, National Research Council, Bologna, Italy	Flybase: FBal0182964
D. melanogaster: lamB^{04643}	D. Andrenacci, National Research Council, Bologna, Italy	Flybase: FBal0008068
D. melanogaster: lamC^{CB04957}	D. Andrenacci, National Research Council, Bologna, Italy	Flybase: FBal0211700
D. melanogaster: lamC^{G00158}	D. Andrenacci, National Research Council, Bologna, Italy	Flybase: FBal0147815
D. melanogaster: UAS-HP1a	W. X. Li, University of Rochester, USA (Larson et al., 2012)	N/A
D. melanogaster: Elav-GAL4,UASsyt-GFP/FM7 P{w[+mW.hs] = GawB}elav [C155], P{w[+mC] = UAS-syt.eGFP}1, w[*]	Bloomington Drosophila Stock Center	BDSC: 6923 Flybase: FBti0002575
D. melanogaster: Rhodopsin1-GAL4;UAS-GFP	B. Mollereau, École Normale Supérieure de Lyon, France	N/A
D. melanogaster: Hecw^{KO}	Fajner et al., 2021	N/A
D. melanogaster: UAS-RFP::Hecw	Fajner et al., 2021	N/A
D. melanogaster: UAS-LBR^{GD2133}	Vienna Drosophila Resource Center	VDRC: 39468
w1118; P{GD2133}v39468		Flybase: FBtp0029702
D. melanogaster: UAS-cpb^{GD9299}	Vienna Drosophila Resource Center	VDRC: 45668
w1118; P{GD9299}v45668		Flybase: FBtp0036026
D. melanogaster: dTAU^{RNAi}	Bloomington Drosophila Stock Center	BDSC: 28891
dTauTRiP.HM05101:y1 v1; P{TRiP.HM05101}attP2		Flybase: FBtp0051189
D. melanogaster: UAS-hTAU (UAS-hTAU^{0N4R})	P. Dourlen	*UAS-hTAU^{0N4R}*
D. melanogaster: UAS-hPIN1	This paper	N/A
M. musculus	Lab Mallamaci	*CD1*
M. musculus (Pin1$^{-/-}$ and wt littermates)	Lab Del Sal	*C57BL/6*
Oligonucleotides		
See Table S3		N/A

(*Continued on next page*)

Continued

REAGENT or RESOURCE	SOURCE	IDENTIFIER
Recombinant DNA		
Vector: pUAST	F. Feiguin Lab	N/A
Plasmid: pUAST-hPIN1	This paper	N/A
Plasmid: pGEX6P1-Hecw WT	Fajner et al., 2021	N/A
Plasmid: pGEX6P1-Hecw C1394W	Fajner et al., 2021	N/A
Plasmid: pET16b-full HP1a-HIS	RIKEN BioResource Research Center	RDB15203
His tagged E1 enzyme Uba1	Addgene	34965
His tagged E2 enzyme Ube2D3	S.Polo Lab	N/A
Software and algorithms		
FIJI software v1.0	https://imagej.net/software/fiji/	RRID:SCR_002285
Zen2 imaging software	Zeiss	Zeiss
FastQC(v0.11.7)	Andrews, 2015	https://www.bioinformatics.babraham.ac.uk/projects/fastqc/; RRID:SCR_014583
Trimmomatic (v0.38)	Bolger et al., 2014	http://www.usadellab.org/cms/index.php?page=trimmomatic; RRID:SCR_011848
STAR (v2.6.0c)	Dobin et al., 2013	https://github.com/alexdobin/STAR; RRID:SCR_004463
DESeq2 (v1.26.0)	Love et al., 2014	RRID:SCR_015687
DAVID software (v6.8)	Huang et al., 2009	RRID: SCR_001881
SQuIRE	Yang et al., 2019	N/A
Samtools (v1.3.1)	Li et al., 2009	https://www.htslib.org/download/; RRID:SCR_002105
Bedtools intersect (v2.27.0)	Quinlan and Hall, 2010	https://github.com/arq5x/bedtools2; RRID:SCR_006646
DIOPT-DRSC Integrative Ortholog Prediction Tool (v8)	Hu et al., 2011	https://www.flyrnai.org/cgi-bin/DRSC_orthologs.pl
Picard FilterSamReads (v2.18.4).	N/A	https://gatk.broadinstitute.org/hc/en-us/articles/360036882611-FilterSamReads-Picard
OpenComet (v1.3.1)	Gyori et al., 2014	https://cometbio.org/
Biorender	N/A	biorender.com
StarDIST	MICCAI, 2018	https://github.com/stardist/stardist; https://imagej.net/plugins/stardist#citation
Other		
Phalloidin-Rhodamine	Life Technologies	Cat#R415; RRID: AB_2572408
Schneider's Drosophila Medium	GIBCO	Cat#21720024
OCT medium	Bio Optica	Cod CND: W01030799
Prolong Gold fluorescence anti-fading reagent	Invitrogen	Cat#P36930
Qiazol	QIAGEN	Cat#79306
A/G PLUS-Agarose resin beads	Santa Cruz Biotech	sc-2003
Glutathione-Sepharose beads	GE Healthcare	N/A
HisPur Ni-NTA resin	Life Technologies	N/A
Superdex 75 size exclusion choursomatography column	GE Healthcare	N/A
Pierce ECL Western reagent	Thermo scientific	Cat#32106
Pierce ECL plus reagent	Thermo scientific	Cat#32132

RESOURCE AVAILABILITY

Lead contact

Further information and requests for resources and reagents should be directed to and will be fulfilled by the lead contact, Giannino Del Sal (gdelsal@units.it).

Materials availability

Materials generated during this study are available from the Lead contact upon request, but we may require a payment and/or a completed Materials Transfer Agreement if there is potential for commercial application.

Data and code availability

Data generated in this study are available within this paper and upon request from the Lead Contact. The RNaseq dataset generated during this study are available at the European nucleotide archive (ENA): PRJEB41707, https://www.ebi.ac.uk/ena/browser/home. The accession numbers for the publicly available datasets analyzed in this paper are listed in the Key resources table.

This paper does not report original code.

Any additional information required to reanalyze the data reported in this work paper is available from the Lead Contact upon request.

EXPERIMENTAL MODEL AND SUBJECT DETAILS

Fly stocks and treatments

The following *Drosophila melanogaster* stocks were used: w^{1118} (kind gift of V. Specchia, University of Salento), $dodo^{EY03779}$ (BDSC#15677), *UAS-dodo* (Kang et al., 2015), $UAS\text{-}dodo^{KK108535}$ (VDRC#110593), $UAS\text{-}Luciferase^{RNAi}$ (BDSC#35788), $lamB^{K2}$ and $lamB^{04643}$ (kind gifts of D. Andrenacci, National Research Council, Bologna, Italy), $lamC^{CB04957}$ and $lamC^{G00158}$ (kind gifts of D. Andrenacci, National Research Council, Bologna, Italy), *UAS-HP1a* (Larson et al., 2012) (kind gift of W. X. Li, University of Rochester, USA), *Elav-GAL4,UASsyt-GFP/FM7* (BDSC#6923), *Rhodopsin1-GAL4;UAS-GFP* (kind gift of B. Mollereau, École Normale Supérieure de Lyon, France), $Hecw^{KO}$ (Fajner et al., 2021), *UAS-RFP::Hecw* (Fajner et al., 2021), $UAS\text{-}LBR^{GD2133}$ (VDRC#39468), $UAS\text{-}cpb^{GD9299}$ (VDRC#45668), $dTau^{TRiP.HM05101}$ (BDSC#28891) and *UAS-hTAU* ($UAS\text{-}hTAU^{0N4R}$, kind gift of P. Dourlen, University of Lille, France). To generate *UAS-hPIN1* transgenic flies, *hPIN1* full cDNA EcoRI/XhoI restriction fragment was cloned in the *pUAST* vector, and the contruct used for standard fly embryo microinjection by BestGene Inc. (USA). All *Drosophila melanogaster* lines were cultured at 25°C on standard corn/yeast flyfood. Experiments were performed in age-matched 4, 14, 21 and 35 days old adult female flies. For 3TC feeding, newborn flies were cultured on flyfood supplemented with 100 μM 3TC (Lamivudine, Sigma-Aldrich, L1295).

Primary cultures

Neocortices from E16.5 wt CD1 mouse embryos were collected, pooled and chopped to small pieces in ice-cold PBS, 0.6% glucose buffer, supplemented with 0.1% DNaseI . The minced tissue was resuspended and incubated in 0.25 mg/ml trypsin, 4 mg/ml DNaseI for 5 minutes at 37°C. Digestion reaction was stopped by adding $\geq$ 1.5 volumes of DMEM-F12, 10% FBS medium. Tissues were spun down and transferred to Neurobasal-A medium, supplemented with Glutamax (GIBCO), B27 (Invitrogen), 25 μM L-glutamate, 25 μM β-Mercaptoethanol, 2% FBS, 10 pg/ml fungizone (GIBCO). Undissociated tissue was sedimented, supernatant harvested and living cells counted. 150,000-200,000 cells/cm^2 were plated in 0.1 mg/ml poly-L-Lysine pre-treated plastic wells and cultured for 8 days, and treated with 5 μM PIB (Calbiochem, 529627) (48 hours single hit or 48+48 hours double hit), 1 μM MG132 (Sigma-Aldrich, 474790) for 16 hours, 100 μM 3TC (Lamivudine, Sigma-Aldrich, L1295) for 48 hours.

Mice

Procedures involving mice and their care were in conformity with national (D.L. 26/2014 and subsequent implementing circulars) and international (EU Directive 2010/63/EU for animal experiments) laws and policies, and the experimental protocol was approved by the Ethical Committee of the University of Trieste and the Italian Ministry of Health (Authorization n. 12/2017-PR). *Wild-type* and $Pin1^{-/-}$ mice were maintained on a C57BL/6 background and genotyping was performed by polymerase chain reaction (PCR) analysis as described (Girardini et al., 2014). Proximity ligation assay, western blot and qPCR experiments were performed in age-matched 8, 12 and 24 months old adult female mice. Immunohistochemistry experiments were performed in age-matched 8 months old adult female and 24 months old adult male mice. Immunofluorescence experiments were performed in age-matched 24 months old adult male mice.

Human brain tissues

Paraffin-embedded enthorinal cortex samples of male sex matched non-demented controls (#1997-143 and 2007-046) and AD patient (#2009-040) were obtained from the Netherlands Brain Bank (NBB), Netherlands Institute of Neuroscience, Amsterdm (https://www.brainbank.nl/). All material has been collected from donors for or from whom a written informed consent for a brain autopsy and the use of material and clinical information for research purposes had been obtained by the NBB.

METHOD DETAILS

Drosophila organ dissection

Flies were ice-anesthetized, heads, brains and ovaries were dissected in Schneider's *Drosophila* Medium (GIBCO, 21720024), supplemented with 10% heat-inactivated FBS and 10 mg/L Insulin (Sigma-Aldrich, I2643).

Drosophila ex-vivo brain culture

Retina was removed from dissected heads, and brains incubated in in Schneider's *Drosophila* Medium (GIBCO,21720024), supplemented with 10% heat-inactivated FBS and 10 mg/L Insulin (Sigma-Aldrich, I2643). For drug treatments, medium was supplemented with DMSO (Sigma-Aldrich, D4540) (control vehicle), 0.2 μM PiB (Calbiochem, 529627) (3h, room temperature), 5 μM KPT6566 (Buxboim et al., 2014) (3h, room temperature), 25 μM MG132 (Sigma-Aldrich, 474790) (3h, room temperature), 50 μM Roscovitine (Sigma-Aldrich, R7772) (3-6h, room temperature), 1 μM Jasplakinolide (Santa Cruz, sc-202191) (3h, room temperature).

Drosophila organ whole mount TUNEL

Drosophila tissues were stained according to a standard protocol (Napoletano et al., 2017). Briefly, organs were fixed in 4% paraformaldehyde (Sigma-Aldrich, 158127) in PBS 15 minutes at room temperature, washed in PBS, permeabilized in PBS 0.1% Triton X-100, 100mM citrate 1 hour at 65°C, washed in PBS, incubated TUNEL reagent (*In situ* cell death detection kit, TMR red, Sigma-Aldrich, 12156792910) 14-16 hours at 37°C, washed in PBS, incubated with HOECHST 33342 (Sigma-Aldrich, B2261, 2 μg/ml in PBS) 10 minutes at room temperature, rinsed in PBS and H_2O at room temperature, and mounted on glass slides with Prolong Gold fluorescence anti-fading reagent (Invitrogen, P36930).

Drosophila organ whole mount immunofluorescence

Drosophila tissues were stained according to a standard protocol (Bertolio et al., 2019). Briefly, organs were fixed in 4% paraformaldehyde (Sigma-Aldrich, 158127) in PBS 15 minutes at room temperature, washed in PBS, permeabilized in PBS 0.1% Triton X-100 1 hour at room temperature, incubated with primary antibodies diluted in PBS 0.1% Triton X-100 14-16 hours at 4°C, washed in PBS 0.1% Triton X-100, incubated with secondary antibodies in PBS 0.1% Triton X-100 2 hours at room temperature, then washed in PBS 0.1% Triton X-100, incubated with HOECHST 33342 (Sigma-Aldrich, B2261, 2 μg/ml in PBS) 10 minutes at room temperature, rinsed in PBS and H_2O at room temperature, and mounted on glass slides with Prolong Gold fluorescence anti-fading reagent (Invitrogen, P36930).

Primary antibodies used were: rabbit anti-hPIN1/Dodo 1:50 (G. Del Sal lab; Zacchi et al., 2002), mouse anti-HP1a C1A9 1:500 (DSHB; AB_528276), rabbit anti-HP1a W11 1:500 (Kind gift of S.C.R. Elgin), mouse anti-LamB ADL67.10 1:500 (DSHB; AB_528336), rat anti-Elav 7E8A10 1:500 (DSHB; AB_528218), guinea pig anti-Sqh1P 1:100 (Kind gift of R.E. Ward; Zhang and Ward, 2011).

Secondary antibodies used were: goat anti-mouse Alexa Fluor 488 A-11001 1:200 (Life Technologies; AB_2534069), goat anti-mouse Alexa fluor 568 A-11004 1:200 (Life Technologies; AB_2534072), donkey anti-mouse Alexa fluor 647 A-31571 1:200 (Life Technologies; AB_162542), goat anti-rabbit Alexa Fluor 488 A-11008 1:200 (Technologies; AB_143165Life), goat anti-rabbit Alexa Fluor 568 A-11011 1:200 (Life Technologies; AB_143157), goat anti-rat Alexa fluor 647 A-21247 1:200 (Life Technologies; AB_141778); goat anti-guinea pig 568 A-11075 1:200 (Life Technologies; AB_2534119).

F-Actin was stained with Phalloidin-Rhodamine R415 (Life Technologies; AB_2572408).

Drosophila tissue cryosections

Dissected flies heads were fixed in 4% paraformaldehyde (Sigma-Aldrich, 158127) in PBS 14-16 hours at 4°C, washed in PBS, equilibrated in 30% sucrose 48-72 hours at 4°C, rinsed in PBS, then embedded in OCT medium (Bio Optica, W01030799) and frozen on isopentane/liquid nitrogen bath. Embedded tissue was cryosectioned in 10 μm thick slices.

Drosophila tissue cryosection TUNEL

Tissue cryosections were permeabilised in PBS 0.1% Triton X-100 100mM citrate 1 hour at 65°C, washed in PBS, incubated TUNEL reagent (*In situ* cell death detection kit, TMR red, Sigma-Aldrich, 12156792910) 14-16 hours at 37°C, washed in PBS, incubated with HOECHST 33342 (Sigma-Aldrich, B2261, 2 μg/ml in PBS) 10 minutes at room temperature, rinsed in PBS and H_2O at room temperature, and mounted on glass slides with Prolong Gold fluorescence anti-fading reagent (Invitrogen, P36930).

Drosophila tissue cryosection immunofluorescence

Drosophila tissue cryosections were stained according to a standard protocol (Napoletano et al., 2011). Briefly, cryosections were permeabilised in PBS 0.1% Triton X-100 100mM citrate 1 hour at 65°C, washed in PBS, incubated 2 hours at room temperature in 3% Fetal Bovin Serum in PBS 0.1% Triton X-100, rinsed in PBS 0.1% Triton X-100, incubated with primary antibodies diluted in 3% Fetal Bovin Serum in PBS 0.1% Triton X-100 14-16 hours at 4°C, washed in PBS 0.1% Triton X-100, incubated with secondary antibodies diluted in 3% Fetal Bovin Serum in PBS 0.1% Triton X-100 2 hours at room temperature, then washed in PBS 0.1% Triton X-100,

incubated with HOECHST 33342 (Sigma-Aldrich, B2261, 2 μg/ml in PBS) 10 minutes at room temperature, rinsed in PBS and H_2O at room temperature, and mounted on glass slides with Prolong Gold fluorescence anti-fading reagent (Invitrogen, P36930).

Primary antibodies used were: rabbit anti-hPIN1/Dodo 1:50 (G. Del Sal lab; Zacchi et al., 2002), mouse anti-HP1a C1A9 1:500 (DSHB; AB_528276), rabbit anti-HP1a W11 1:500 (Kind gift of S.C.R. Elgin), mouse anti-LamB ADL67.10 1:500 (DSHB; AB_528336), rat anti-Elav 7E8A10 1:500 (DSHB; AB_528218), guinea pig anti-Sqh1P 1:100 (Kind gift of R.E. Ward; Zhang and Ward, 2011).

Secondary antibodies used were: goat anti-mouse Alexa Fluor 488 A-11001 1:200 (Life Technologies; AB_2534069), goat anti-mouse Alexa fluor 568 A-11004 1:200 (Life Technologies; AB_2534072), donkey anti-mouse Alexa fluor 647 A-31571 1:200 (Life Technologies; AB_162542), goat anti-rabbit Alexa Fluor 488 A-11008 1:200 (Technologies; AB_143165Life), goat anti-rabbit Alexa Fluor 568 A-11011 1:200 (Life Technologies; AB_143157), goat anti-rat Alexa fluor 647 A-21247 1:200 (Life Technologies; AB_141778); goat anti-guinea pig 568 A-11075 1:200 (Life Technologies; AB_2534119).

F-Actin was stained with Phalloidin-Rhodamine R415 (Life Technologies; AB_2572408).

Proximity ligation assay (PLA) in *Drosophila* tissue

Proximity ligation assay (PLA) was performed using Duolink *in situ* Red Starter Kit Mouse/Rabbit (Sigma Aldrich, DUO92101) according to the manufacturer's protocol.

Primary antibodies used were: rabbit anti-hPIN1/Dodo 1:50 (G. Del Sal lab; Zacchi et al., 2002), mouse anti-LamB ADL67.10 1:500 (DSHB; AB_528336).

COMET assay in *Drosophila* tissue

Alkaline COMET assay was performed on a single cell fly brain suspension, using CometAssay Reagent Kit for Single Cell Gel Electrophoresis Assay (Trevigen, 4250-050-K), according to the manufacturer protocol. All the instruments and equipment required for preparation of this suspension was coated with ice-cold coating solution (1% BSA in Ca^{2+} and Mg^{2+} free PBS) and kept on ice. 4 days old female flies were ice-anesthetized, and brains were dissected in ice-cold Schneider's *Drosophila* Medium (GIBCO, 21720024), supplemented with 10% heat-inactivated FBS and 10 mg/L Insulin (Sigma-Aldrich, I2643), on ice. For each sample, a pool of n = 20 dissected brains was washed and resuspended in 400 μL ice-cold Ca^{2+} and Mg^{2+} free PBS, and kept on ice. Brains were then gently homogenized in ice-cold 2 mL tissue Glass Grinder, with 10 slow strokes, triturated through five-times resuspension with fire-narrowed (to approximately 50% tip diameter) tip ice-cold glass Pasteur pipette, to obtain a single cell suspension, and kept on ice. The cell suspension was then filtered through ice-cold 40 μm cell strainer, and kept on ice. The required ell concentration (150000 viable cells/ml) was verified by quantification of Tyrpan blue-negative cells, using a Burker chamber. Irradiated samples were obtained by 5 Gy γ-irradiation. Cell suspensions were then analyzed by agarose gel electrophoresis (N = 3 replicates/condition). Images were acquired using a Olympus BX51 microscope, and comets Tail momentum and Olive momentum quantified using the OpenComet software v1.3.1 (https://cometbio.org/; Gyori et al., 2014).

Drosophila photoreceptor live imaging

GFP-marked outer photopreceptors were visualized according to cornea neutralization protocol (Van Den Brink et al., 2018; Robin et al., 2019). Briefly, ice-anesthetized flies were half-embedded in 1% agarose in a 35 mm cell culture plastic dish, covered with ice-cold H_2O, and observed by fluorescence microscopy using a 40x water immersion lens.

Fly negative geotaxis assay

5 flies/vial gently tapped at the bottom of the vial and then the number of flies that climbed at least 5 cm of the vial wall in 9 s was scored.

Fly fertility assay

Single wild-type (w^{1118}) virgin female flies were mated to single wild-type (w^{1118}) and *dodo* mutant ($dod^{EY03779}$) male. Mated females laid eggs for 6 days. Ten replicate crosses were set for each condition. The number of pupae emerging from each tube was scored.

Fly learning and memory assays

The learning assay was adapted from an assay described in Seugnet et al. (2009). We used a T maze system in which the apparatus contained two horizontal 14 cm cylindrical tubes, separated by an opaque and mobile window: one tube was kept in the dark by covering it with a non-transparent layer, the second one was lighted up. For each condition, n = 5 groups (N = 20 individuals/group) were assayed for the ability to associate light with a negative stimulus (quinine bitter taste) that inhibits phototaxis (aversive learning). The lighted up tube contained a piece of filter paper soaked with 0.1M quinine solution. Each fly group was placed at the bottom of the dark tube and acclimated for 30 s in dark conditions before opening the window to allow entry in the lighted up tube. Flies entered in the lighted up tube (positive to the phototaxis) was re-tested. Each group was trained in the same conditions for 5 times. For each test, the fractions of individuals entering (unlearned) or avoiding (learning) the lighted up tube were calculated. Filter papers and tubes were replaced between each test. To analyze short-term memory, single groups of trained flies were left for 5 hours at 25°C and re-tested. The fractions of individuals entering (memory-defective) or avoiding (memorizing) the lighted up tube were calculated.

Immunohistochemistry of analysis of mouse and human tissue sections

Post mortem collected tissues from wt and *Pin1*$^{-/-}$ mice (Girardini et al., 2011) were fixed in 10% neutral buffered formalin for 14-16 hours, washed in H_2O and paraffin-embedded. Paraffin-embedded mouse and human tissue 2.5-3 μm thick slices were sectioned, dried, de-waxed and rehydrated. The antigen unmasking technique was performed using Target Retrieval Solutions at pH6 or pH9 30 minute at 98°C. After neutralization of the endogenous peroxidase with 3% H_2O_2 and blocking, slices were incubated with primary antibodies 14-16 hours at 4°C and washed in 0.1% Triton X-100 PBS. IHC staining was revealed using DAB (3,3′-diaminobenzidine) as chromogen substrate.

Primary antibodies used were: rabbit anti-hPIN1/Dodo 1:100 (G. Del Sal lab; Zacchi et al., 2002), rabbit anti-LamB1 ab16048 1:1000 (Abcam; AB_443298), mouse anti-LamB1 ab8982 1:1000 (Abcam; AB_1640627), mouse anti-LamA/C sc-7292 1:100 (Santa Cruz; AB_627875), rabbit anti-γH2AX ab11174 1:1000 (Abcam; AB_297813), rabbit anti-pChk1 ab58567 1:500 (Abcam; AB_10563825), rabbit anti-53BP1 NB100-304 1:1000 (Novus; AB_10003037), mouse anti-H3K9me2 ab1220 1:1000 (Abcam; AB_449854).

Secondary antibodies used were: donkey anti-rabbit IgG 1:500 (Novex by Life Technologies), rabbit anti-mouse IgG 1:200 (Sigma-Aldrich).

Immunofluorescence analysis of mouse and human tissue sections and mouse primary neuronal cultures

Mouse dissected tissue were fixed formalin and paraffin-embedded. Mouse and human 2.5-3 μm thick slices were sectioned, de-waxed and rehydrated. The antigen unmasking technique was performed using Target Retrieval Solutions at pH6 or pH9 30 minute at 98°C. After blocking, slices were incubated with primary antibodies for 14-16 hours at 4°C and washed in 0.1% Triton X-100 PBS. Neuronal cells cultured on glass slides were fixed in 4% paraformaldehyde for 15 minutes at room temperature, washed in PBS, permeabilized in 0.1% Triton X-100 PBS for 1 hour at room temperature, incubated with primary antibodies diluted in 0.1% Triton X-100 PBS for 14-16 hours at 4°C.

Tissues and cells were then washed in 0.1% Triton X-100 PBS, incubated with secondary antibodies in 0.1% Triton X-100 PBS for 2 hours at room temperature, then washed in PBS 0.1% Triton X-100, incubated with HOECHST 33342, for 10 minutes at room temperature, rinsed in PBS and H_2O at room temperature, and mounted on glass slides with Prolong Gold fluorescence anti-fading reagent.

Primary antibodies used were: rabbit anti-LamB1 ab16048 1:1000 (Abcam; AB_443298), mouse anti-LamB1 ab8982 1:1000 (Abcam; AB_1640627), mouse anti-LamA/C sc-7292 1:100 (Santa Cruz; AB_627875), mouse anti-H3K9me2 ab1220 1:1000 (Abcam; AB_449854), and mouse anti-βIII-Tubulin.

Secondary antibodies used were: goat anti-mouse Alexa Fluor 488 A-11001 1:200 (Life Technologies; AB_2534069), goat anti-mouse Alexa fluor 568 A-11004 1:200 (Life Technologies; AB_2534072), goat anti-rabbit Alexa Fluor 488 A-11008 1:200 (Technologies; AB_143165Life), goat anti-rabbit Alexa Fluor 568 A-11011 1:200 (Life Technologies; AB_143157).

Proximity ligation assay (PLA) assay in mouse tissue

Proximity ligation assay (PLA) was performed using Duolink *in situ* Red Starter Kit Mouse/Rabbit (Sigma Aldrich, DUO92101) according to the manufacturer's protocol.

Primary antibodies used were: mouse anti-Lamin B1 sc-373918 1:100 (Santa Cruz; AB_10945297, clone G-1), rabbit anti-HP1α ab109028 1:100 (Abcam; AB_10858495, clone EPR5777).

Image acquisition and analysis

For analyses of *Drosophila* tissues and mouse brain neocortical primary neuronal cultures, images were acquired using a Nikon ECLIPSE C1si confocal microscope (Confocal Microscopy Unit, University of Trieste, Italy). Super-resolution images were acquired using a Leica SP8 LIGHTNING confocal microscope (Imaging Unit, IFOM, Milan, Italy).

Analysis of mouse and human tissue sections was performed with a Zeiss AXIO Scope.A1 microscope, and microphotographs were collected using a Zeiss Axiocam 503 Color digital camera using the Zen2 imaging software (Zeiss).

Graphical abstract was created using Biorender, with publishing license to F.N.

Total RNA and genomic DNA purification

RNA purification from tissues and cells was performed using Qiazol (QIAGEN, 79306) reagent according to manufacturer's protocol. For *Drosophila*, tissues from 5-10 female flies per sample were pooled. Fly samples were manually lysed using a pestle. Mouse samples were homogenized using the gentle Octo Dissociator (Miltenyi Biotec).

For genomic DNA (gDNA) purification, tissues from 30 female flies per sample were pooled, manually lysed using a pestle in 0.1M Tris HCl pH9.0, 0.1M EDTA, 1% SDS buffer, and gDNA purified using Phenol/chloroform extraction and alcoholic precipitation.

Paired end sequencing of *Drosophila* head RNA and analyses

Tissues from 30 female flies per sample were pooled. Purified RNA (RIN > 7.5) was sequenced by Biodiversa s.r.l. (Rovereto, Italy). RNA library was prepare using RiboZero kit (Illuina) and samples sequenced using Illumina HiSeq platform and (2x150 bb strand-specific reads, for a total of 80M reads. For analysis of sequenced RNA, reads quality and adaptor content were assessed using FastQC

(v0.11.7) (https://www.bioinformatics.babraham.ac.uk/projects/fastqc/) (Andrews, 2015). Adapters were removed using Trimmomatic (v0.38) (Bolger et al., 2014) (http://www.usadellab.org/cms/index.php?page=trimmomatic) with default parameters except for the minimum read length threshold, which was set to 50 (MINLEN:50). To perform gene expression analysis, trimmed reads were mapped on the *Drosophila melanogaster* reference genome (BDGP6.22 version) downloaded from Ensembl (Zerbino et al., 2018) (http://www.ensembl.org//useast.ensembl.org/index.html?redirectsrc=//www.ensembl.org%2Findex.html) using STAR (v2.6.0c) (Dobin et al., 2013) (https://github.com/alexdobin/STAR) with default parameters. Gene expression levels were quantified taking advantage of the read counting module embedded within the STAR tool (–quantMode GeneCounts). Differentially expressed genes (DEGs) were identified using DESeq2 (v1.26.0) (Love et al., 2014), estimating size factors with the default median ratio method, estimating the dispersion for negative binomial distributed data and testing for significance with the Wald test. Benjamini & Hochberg false discovery rate (FDR) was then applied to the calculated p value and genes showing FDR < 0.01 were considered as differentially expressed. Gene Ontology and KEGG pathways enrichment analysis were performed with the DAVID software v6.8 (Huang et al., 2009).

TE locus specific expression levels were calculated using SQuIRE (Yang et al., 2019) (https://github.com/wyang17/SQuIRE). First, the reference genome and the annotation datasets referring to the *Drosophila melanogaster* dm6 genome version were downloaded and prepared for the subsequent analyses using the SQuIRE Fetch and Clean modules, then the trimmed reads were mapped on the reference genome using the Map module and finally read counts were estimated using the Count module (strandedness = '1'). TE loci showing concordance between element annotation and read mapping strands (TE_strand and tx_strand) were selected. Elements annotated as artifacts, low_complexity, RNA, satellite, simple_repeat or rRNA were discarded and differentially expressed TE loci were identified using DESeq2. TE loci showing FDR < 0.05 and $\log_2$FC < −1 or > 1 were considered as differentially expressed.

In order to summarize the expression levels of specific TE consensus a method previously discussed in Ansaloni et al., 2019 was used. Briefly, a reference transcriptome was built merging the RepBase TE sequences (Bao et al., 2015) and the Ensembl transcript sequences containing all the coding and non-coding annotated transcripts. Reads were mapped on the reference transcriptome using STAR (v2.6.0c) (Dobin et al., 2013) and assigned primary alignment flag to all the alignments with the best score. All alignments flagged as primary (−F 0 × 100 parameter) were selected using samtools (v1.3.1) (Li et al., 2009) (https://www.htslib.org/download/). To avoid counting reads mapping on TE fragments embedded in coding and/or long non-coding transcripts, reads mapping with best-scoring alignments on any Ensembl transcript were discarded using Python scripts and Picard FilterSamReads (v2.18.4) (https://gatk.broadinstitute.org/hc/en-us/articles/360036882611-FilterSamReads-Picard). Selected reads mapping exclusively on TEs and in the proper orientation were finally counted in each sample. Raw counts were normalized on the total number of mapping reads and multiplied by 1,000,000 (reads per million mapped reads, RPM). To identify TE consensus elements differentially expressed in *dodo* mutant versus control samples (Table S1), two-sided Welch t-Test was applied to RPM normalized counts. Benjamini & Hochberg false discovery rate (FDR) was then applied to the calculated p value and TE consensus showing FDR < 0.05 and $\log_2$FC < −1 or > 1 were considered as differentially expressed.

Analysis of TE loci and gene chromatin states in mature neurons

To calculate the fraction of overlap between TE and gene loci and genomic loci mapped to mature neurons chromatin states, as previously defined by Marshall and Brand (2017), genomic coordinates of annotated TEs and genes, up- and downregulated in *dodo* mutant versus control samples, have been intersected with chromatin state genomic coordinates using bedtools v2.27.0 (Quinlan and Hall, 2010) (https://github.com/arq5x/bedtools2). TEs not overlapping any of the annotated chromatin states have been considered as overlapping the "Not annotated" state. Custom python script has then been used to select the longest intersection in case of TEs overlapping more than one chromatin states. Finally, positive enrichments of up and downregulated TEs respect to the annotated TEs in each of the annotated chromatin states have been tested using Fisher test. Significance threshold was set to P value < 0.001.

PIN1/HP1α signature and human sample dataset analysis

To identify the signature of PIN1-dependet HP1α-repressed genes, human orthologs of *dodo* mutant versus wt flies DEGs from brain RNaseq, which were targets of HP1a (according to DamIDseq coordinates from Marshall and Brand (2017), were identified using DIOPT-DRSC Integrative Ortholog Prediction Tool (Hu et al., 2011) (v8; https://www.flyrnai.org/cgi-bin/DRSC_orthologs.pl). Genes with best DIOPT score in forward and/or reverse mapping were selected. Next, the best rank mapping as well as the highest DIOPT and weighted scores were manually curated to prioritize the best orthologous gene pairs (Table S1). This led to the identification of a PIN1/HP1α signature of 310 human orthologs of genes that were upregulated in *dodo* mutant versus wt flies. For the analysis of this signature expression in human samples, expression data belonging to human control and AD parahippocampal gyrus (BM36-PHG) samples from Mount Sinai Bank study (MSBB) (https://www.synapse.org/#!Synapse:syn8484987) were obtained by accessing the AMP-AD portal (https://adknowledgeportal.synapse.org). Samples with RIN score higher than 5.0 were included in the analysis. The average expression (logCPM) of PIN1/HP1α signature gene, in the patients grouped by CDR (CDR = 0, no cognitive impairment (NCI); CDR = 0.5, mild cognitive impairment (MCI); CDR > 1, Dementia) and Braak stages, was plotted using the R pheatmap package. All statistical analyses were performed within the R environment v3.6.2.

PIN1 expression quantification in AD transcriptomic datasets

To quantify the expression of PIN1 in Alzheimer's Disease patients, in which deregulation of TEs has been previously observed (Guelen et al., 2008; Sun et al., 2018), data from the AMP-AD portal (https://adknowledgeportal.synapse.org) was obtained for the Religious Orders Study and Rush Memory and Aging Project (ROSMAP; https://www.synapse.org/#!Synapse:syn3388564) and The Mayo Clinic Brain Bank (MCBB, https://www.synapse.org/#!Synapse:syn23568549) studies. Totally, raw gene expression levels from dorsolateral prefrontal cortex of 157 AD patients and 87 controls were retrieved from the former (Guelen et al., 2008) whereas expression levels from temporal cortex of 80 AD and 21 controls were retrieved from the latter (Sun et al., 2018). To estimate whether PIN1 was differentially expressed, in AD compared to healthy patients, in both datasets, DEG analysis was performed by using DESeq2 (Love et al., 2014).

Correlation between PIN1 and TEs expression in AD transcriptomic datasets

To correlate the expression levels of PIN1 and TEs, the expression levels of the 12 TEs resulting significantly upregulated in AD versus controls were retrieved from (Sun et al., 2018) (80 AD and 20 controls from the Mayo dataset. Then, a pairwise correlation analysis between the 12 upregulated TEs and the PIN1 gene was done by using the Pearson correlation test. Significant were considered the TE/PIN1 pairs showing an FDR (Benjamini & Hochberg) corrected P value < 0.05.

cDNA synthesis

For gene expression analysis by reverse transcript-quantitative PCR (RT-qPCR), 500 ng of purified total RNA (25ng/μL) were used for RT with the QuantiTect Reverse Transcription kit (QIAGEN, 205313).

Chromatin IP from *Drosophila* tissues

Drosophila heads were dissected in Schneider's Medium (GIBCO, 21720024), supplemented with 10% heat-inactivated FBS and 10 mg\ml Insulin (Sigma-Aldrich, I2643). For each sample, a pool of 120 female heads was incubated in 1 mL of 2% formaldehyde (Sigma-Aldrich, 47608) 20 minutes at room temperature in agitation, and washed in PBS. Next, heads were manually homogenized in 200 μL a buffer composed by 0.1% SDS, 2 mM EDTA, 20 mM Tris pH8.1, and supplemented with protease inhibitor cocktail (CLAP, Sigma-Aldrich, P8340), 1 mM PMSF (Sigma-Aldrich, 78830), 1 mM NaF (Sigma-Aldrich, S7920) and 1 mM Na3VO4 phosphatase inhibitors (Sigma-Aldrich, S6508) (Lysis buffer), diluted by adding 1.8 mL of Lysis buffer and incubated 20 minutes at 4°C in agitation. To shear chromatin, diluted lysates was iteratively (seven times) sonicated with 30 s on/30 s off n = 15 high-power cycles, with a Bioruptor sonicator (Diagenode). The quality of sheared chromatin was checked by 1% agarose gel electrophoresis of a 1/200 sample aliquot, to verify chromatin shearing in 500-1000 bp fragments. Then, each lysate was cleared from debris by for 10 minutes at 18000 *rcf.* centrifugation at 4°C and supernatant diluted with ¼ volume (500 μl) of Dilution buffer (5% Triton X-100, 750 mM NaCl). The diluted sheard chromatin DNA was quantified using a Nanodrop (Thermofisher) spectrophotometer, and diluted to 100 ng/μl with a buffer composed of 0.08% SDS, 1.6 mM EDTA, 16 mM Tris pH8.1, 150 mM NaCl, 1% Triton X-100, supplemented with protease inhibitor cocktail (CLAP, Sigma-Aldrich, P8340), 1 mM PMSF (Sigma-Aldrich, 78830), 1 mM NaF (Sigma-Aldrich, S7920) and 1 mM Na3VO4 phosphatase inhibitors (Sigma-Aldrich, S6508) (IP buffer), and 5 μg saved as "input" fraction. 1 mL chromatin aliquots were then with either 2 μg antibody (IP sample) or no antibody ("resin" sample) incubated 14-16 hours at 4°C in agitation, and then with protein A/G PLUS-Agarose resin beads (Santa Cruz Biotech, sc-2003) 1 hour at 4°C in agitation. Beads-bound chromatin was then isolated by 1 minute 956 *rcf.* centrifugation at 4°C and washed twice with IP buffer, twice with 2 times in IP buffer supplemented with 350mM NaCl, once with 10 mM Tris-HCl pH8, 1 mM EDTA, 250 mM LiCl, 0.5% Na-Deoxycholate, 0.5% NP40 buffer, and washed once and resuspended in a 100 μL aliquot of 10 mM Tris pH8, 1mM EDTA pH8 buffer. Each sample was then incubated with 2 Units DNase-free RNase (Sigma-Aldrich, 556746) for 30 minutes at 37°C, and with 300 mg/ml Proteinase K (Life Technologies, 25530049) in 0.5% SDS, 100 mM NaCl buffer for 14-16 hours at 68°C, to reverse crosslinks. After DNA purification by phenol-chloroform extraction and ethanol precipitation, each DNA sample was resuspended in 400 μL H_2O. A 1/80 aliquot of this purified DNA was used for each qPCR reaction.

Antibodies used were: rabbit anti-H3K9me3 C15410056 (Diagenode), rabbit anti-H3K27me3 C15410195 (Diagenode; AB_2753161, Lot. A0821D and A1811-001P), rabbit anti-H3K9ac 07-352 (Millipore; AB_310544)

Real time quantitative PCR

cDNA (from 25 ng RNA/sample) for reverse transcript-quantitative PCR (RT-qPCR) or gDNA (1/80 purified DNA/sample for ChIP-qPCR and 1.6 ng/sample for CNV assays) were used as templates for real-time qPCR. SYBR Green-based qPCR was performed using the iTaq Universal SYBR Green Supermix (BIO-RAD, 1725125). Taqman-based qPCR was performed using the iQ Multiplex Powermix (BIO-RAD, 172-5849). SYBR Green-based and Taqman qPCR assays were performed using aa BIORAD CFX96 Touch Real-Time PCR Detection System thermocycler. Quantification was based on the $2^{-\Delta\Delta Ct}$ method using the housekeeping *rp49* and *actin*, *DMRT1C*, or *GAPDH* genes as reference.

Protein IP

Tissues and cells were manually lysed in 20 mM Tris-HCl pH8, 150 mM NaCl, 0.2% NP-40, 0.2% Triton X-100, 5 mM EDTA lysis buffer, supplemented with protease and phosphatase inhibitors (1mM NaF Sigma-Aldrich S7920, 1mM PMSF Sigma-Aldrich

78830, 0.1 mM CLAP Sigma-Aldrich P8340, 1mM Na_3VO_4 Sigma-Aldrich S6508), then sonicated on ice, incubated 3h 4°C, and centrifuged 10 minutes 13000 rpm. 5% superrnatant was stored for "input" analysis, the remaining superrnatant was incubated with antibodies 14-16 hours at 4°C, then incubated with protein G beads 1 hour at 4°C and centrifuged 2 minutes 956 r*cf.* Pellets were washed in lysis buffer and the immunocomplex was eluted in Laemmli Buffer and analyzed by SDS-PAGE. For *Drosophila*, tissues from 80 female flies per sample were pooled. For treatment of head protein lysates with λ-protein Phosphatase (Sigma-Aldrich; P9614), lysates were incubated according to the manufacturer protocol.

Antibodies (2μg/reaction) used were: rabbit anti-hPIN1/Dodo (G. Del Sal lab; Zacchi et al., 2002), mouse anti-HP1a C1A9 (DSHB; AB_528276), mouse anti-HA 12CA5 (Boehringer Mannheim), mouse anti-LamB ADL67.10 (DSHB; AB_528336).

Protein purification

Tissues and cells were manually lysed in 20 mM Tris-HCl pH8, 150 mM NaCl, 0.2% NP-40, 0.2% Triton X-100, 5 mM EDTA buffer, supplemented with protease and phosphatase inhibitors (1mM NaF Sigma-Aldrich S7920, 1mM PMSF Sigma-Aldrich 78830, 0.1 mM CLAP Sigma-Aldrich P8340, 1mM Na_3VO_4 Sigma-Aldrich S6508), and with Laemmli Buffer, then sonicated and boiled (5 minutes at 95°C). For *Drosophila*, tissues from 15 female flies per sample were pooled. Mouse samples were homogenized using the gentle MACSTM Octo Dissociator of the Miltery Biotec.

Western blot

Immunoprecipitated and purified proteins were analyzed by SDS-PAGE. For the subsequent transfer of proteins on nitrocellulose membrane the semidry transfer cell (BIORAD) was used. The transfer buffer was composed by 48 mM Tris, 39 mM glycine, 4.13 mM SDS, 20% w/v methanol. After 30 minutes incubation of nitrocellulose membrane in blotto tween (5% milk, 0.2% Tween20 in PBS), the membranes were incubated with the primary antibodies diluted in blotto tween 2 hours at room temperature or 14-16 hours at 4°C. Membranes were then rinsed in PBS, incubated with the HRP-conjugated secondary antibodies for 1 hour at 4°C, washed in PBS, and signal was revealed with ECL (Thermo scientific, 32106) or ECL plus (Thermo scientific, 32132) reagents.

Primary antibodies used were: home made rabbit anti-hPIN1/Dodo 1:500, (G. Del Sal lab; Zacchi et al., 2002), mouse anti-HP1a C1A9 1:2000 (DSHB; AB_528276), rabbit anti-HP1a W11 1:500 (Kind gift of S.C.R. Elgin), mouse anti-LamB ADL67.10 1:2000 (DSHB; AB_528336), mouse anti-LamC LC28.26 1:2000 (DSHB; AB_528339), mouse anti-γH2Av UNC93-5.2.1 1:500 (DSHB; AB_2618077), mouse anti-Hecw 1:250 (S. Polo lab; Fajner et al., 2021), rabbit anti-Actin A2066 1:2000 (Sigma; AB_476693), rabbit anti-H3K9me3 C15410056 1:2000 (Diagenode), rabbit anti-LamB1 ab16048 1:2000 (Abcam; AB_443298), mouse anti-LamB1 ab8982 1:2000 (Abcam; AB_1640627), mouse anti-HP1α 05-689 1:2000 (Millipore; AB_11213599), rabbit anti-HP1α ab109028 1:2000 (Abcam; AB_10858495), mouse anti-Ubiquitin ZTA10 (S. Polo lab), rabbit anti-Histone H3 ab1791 1:10000 (Abcam; AB_302613), rabbit anti-γH2AX ab11174 1:500 (Abcam; AB_297813) mouse anti-H3K9me2 ab1220 1:1000 (Abcam; AB_449854) rabbit anti-TAU GTX112981 1:1000 (Gene Tex).

Secondary antibodies used were: goat anti-mouse HRP A90-516P 1:2000 (Bethyl; AB_10631212), goat anti-rabbit HRP A120-201P 1:2000 (Bethyl; AB_67265).

In vitro assays

pGEX6P1-Hecw WT and C1394W mutant were generated by site-directed mutagenesis (Fajner et al., 2021). pET16b-full HP1a-HIS clone was obtained from RIKEN BioResource Research Center. Expression constructs for the Ubch5c and E1 were already described in Maspero and Polo (2016). All constructs were sequence verified.

GST fusion proteins were expressed in Rosetta cells (Novagen) for 16 hours at 18°C after induction with 500 μM IPTG at 0.5 OD_{600}. Cell pellets were resuspended in 50 mM Na-HEPES, pH 7.5, 200 mM NaCl, 1 mM EDTA, 0.1% NP40, 5% glycerol buffer, supplemented with Protease Inhibitor Cocktail set III (Calbiochem). Sonicated lysates were cleared by centrifugation at max speed for 45 minutes. Supernatants were then incubated with glutathione-Sepharose beads (GE Healthcare) 4 hours at 4°C. Beads were then washed with PBS and equilibrated in maintenance buffer (50 mM Tris-HCl, pH7.4, 100 mM NaCl, 1mM EDTA, 1mM DTT, 10% glycerol).

His tagged E1 enzyme Uba1 (Addgene clone #34965) was produced in Rosetta cells. His tagged E2 enzyme Ube2D3 (UBCH5c) was expressed in BL21 cells for 16 hours at 18°C after induction with 1 mM IPTG at 0.6 OD_{600}. Cell pellets were resuspended in 50 mM NaH_2PO_4 pH7.8, 300 mM NaCl, 10% glycerol, 10 mM imidazole buffer (buffer A), supplemented with protease inhibitors, and lysed by sonication. Cell debris was removed by centrifugation and the supernatant incubated with 1 mL of HisPur Ni-NTA resin (Life Technologies) 2 hours at 4°C. Beads were then washed with Buffer A, Buffer A + 1M NaCl, and Buffer A + 20 mM imidazole. His-Ube2D3 protein was eluted in Buffer A + 300 mM imidazole. After overnight dialysis in Size Exclusion Buffer, Ube2D3 was purified onto a Superdex 75 size exclusion chromatography column (GE Healthcare).

His tagged HP1a was expressed in Rosetta for 16 hours at 18°C after induction with 1 mM IPTG at 0.6 OD_{600}. Cell pellets were resuspended in Buffer A and lysed by sonication. Cell debris was removed by centrifugation and the supernatant incubated with 1 mL of HisPur Ni-NTA resin (Life Technologies) 2 hours at 4°C. Beads were then washed with Buffer A, Buffer A + 1 M NaCl, and Buffer A + 20 mM imidazole. Beads-conjugated HP1a-His was used for Ubiquitination assay.

Untagged WT Ubiquitin from Sigma was resuspended in maintenance buffer (50 mM Tris-HCl, pH 7.4, 100 mM NaCl, 1mM EDTA, 1mM DTT, 10% glycerol) and purified onto a Superdex 75 size exclusion chromatography column (GE Healthcare).

Ubiquitination assays were performed with full-length Hecw WT and C1394W mutant produced as GST fusion proteins. Reaction mixtures contained purified enzymes (20 nM E1, 250 nM Ube2D3, 250 nM GST-Hecw), 1.2 μM substrate (NiNTA bound HP1a-His) and 2.5 μM WT or mutant Ubiquitin in ubiquitination buffer (25 mM Tris-HCl, pH7.6, 5 mM MgCl2, 100 mM NaCl, 0.2 μM DTT, 2 mM ATP) and were incubated 60 minutes at 30°C. Samples were then centrifuged to obtain pellets, containing ubiquitinated substrates, and supernatants, containing the enzymes and the soluble Ubiquitin chains. Pellet was washed in 50 mM Tris-HCl pH7.4, 300 mM NaCl, 0.1% Triton X-100, 5% glycerol, 1M UREA buffer and analyzed by SDS-PAGE gel.

After immunoblotting, Coomassie-stained membrane were used to control protein loads.

Oligonucleotides used in this study

List of oligonucleotides used in this study is included in Table S3.

QUANTIFICATION AND STATISTICAL ANALYSIS

Statistical details of experiments can be found in figure, figure legends and method section.

For quantification of LamB and LamB1 invaginations in *Drosophila* tissues and mouse brain neocortical primary neuronal cultures images, the fraction of cells with LamB and LamB1 invaginations was manually scored and computed using the FIJI software (https://imagej.net/software/fiji/). Quantification of nuclear envelope size, based on LamB staining, in the fly brain, was manually performed using the FIJI software (https://imagej.net/software/fiji/). Quantification of nuclear circularity and area based on HOECHST staining in the fly brain was performed through the StarDIST software (https://github.com/stardist/stardist; https://imagej.net/plugins/stardist#citation) (MICCAI, 2018), in collaboration with the IFOM Imaging Unit (Milan, Italy).

Morphometric analyses of nuclear Lamin proteins in mouse and human tissue sections were performed thoursough a MATLAB-developed methodology requiring about a second to segment a truecolor image of 1932*1460 pixels on a mid-range personal computer, and based on the so-called trous algorithm (Guastella and Valenti, 2016), to extracts all main components and reduce noise. The structures of the fifth wavelet plane, with at least 1600 pixels and 30% of blue relative to their areas, were considered. These pre-defined values were determined on an extended experimental basis. The nuclear fractal measure was computed as the ratio between area and perimeter (circularity) of each structure.

Quantifications of western blots were performed by densitometric analysis using Fiji software, and show mean values ± SD of N = 3 biological replicates.